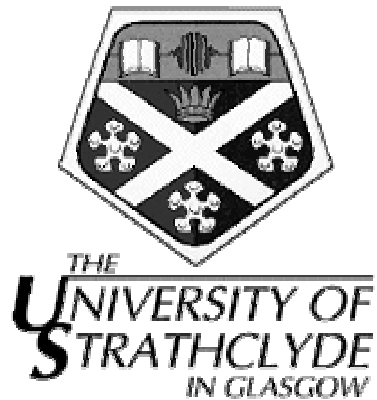# *INTER-COMPARISON OF MEDICAL IMAGE SEGMENTATION ALGORITHMS*

Pujari Amit Narahar

MSc - 2005/06

Bio-Engineering Department

ACKNOWLEDGEMENTS

ABSTRACT

Segmentation of images is a vital part of medical image processing, and MRI (Magnetic Resonance Imaging) is already recognized as a very important tool for clinical diagnosis. In this thesis, comparisons between different segmentation algorithms are carried out, specifically on brain MRI images. Initial parts of the thesis provide the background to the project, and an introduction to the basic principles of MRI, respectively, followed by parameter definitions and MRI image artifacts. The next part briefly covers various image pre-processing techniques which are required, and this is followed with a review of the major segmentation techniques which are available, including thresholding, region growing, clustering, and K-Means clustering. The concept of fuzzy logic is also introduced here, and the chapter concludes with a discussion of fuzzy logic based segmentation algorithms such as Fuzzy C-Means (FCM) and Improved Fuzzy C-Means (IFCM) clustering algorithms. The following part provides details concerning the source, type and parameters of the data (images) used for this thesis. Evaluation and inter-comparisons between a number of different segmentation algorithms are given in near concluding part, finally, conclusions and suggestions for future research are provided in last part.

Qualitative comparisons on real images and quantitative comparisons on simulated images were performed. Both qualitative and quantitative comparisons demonstrated that fuzzy logic based segmentation algorithms are superior in comparison with classical segmentation algorithms. Edge-based segmentation algorithms demonstrated the poorest performance of all; K-means and IFCM clustering algorithms performed better, and FCM demonstrated the best performance of all. However, it should be noted that IFCM was not properly evaluated due to time restrictions in code generation, testing and evaluation.

CONTENTS

Chapter 3

MR IMAGE PREPROCESSING…………………………………………………………**20**

Chapter 4

MR IMAGE SEGMENTATION………………………………………………………..**22**

Chapter 5

DATA COLLECTION…………………………………………………………………..**37**

Chapter 6

Chapter 7

CHAPTER 1

INTRODUCTION

1.1 BACKGROUND

There is tremendous increase in the importance of automated computer techniques in medical image analysis. One of the reasons of increased importance of automated computer analysis can be given as, manual analysis is too time consuming. Apart from time consumed, quality of manual image analysis also depends upon workload and other factors; such as more than one human operator can degrade the quality of analysis and large amount of work can also decrease the accuracy of analysis.

Because of above-mentioned and many other technical reasons there is obvious surge in automated computer (medical) analysis methods. And in the analysis of medical images, segmentation is an imperative process. So along with the developments in automated computer analysis methods, there has been large amount of research carried out in the design and development of image segmentation algorithms. Various segmentation algorithms have been proposed over the years by many researchers.

Due to availability of number of segmentation algorithms based on various techniques like classical, fuzzy, and statistical; there seems to be obvious need for evaluation and comparison of different segmentation algorithms. As inter comparison between different segmentation algorithms facilitates good insight into performances of those algorithms. By observing performances of different segmentation algorithms for similar inputs, evaluation of them is possible. Objective of this thesis is inter-comparison of different (medical) image segmentation algorithms.

For testing the performance of different segmentation algorithms only brain images were used in this thesis. Particularly brain images were used since, brain image possesses most complex anatomical details, therefore for evaluation of

segmentation algorithms in segmenting medical images, brain image can be said as best choice.

The main brain imaging techniques include Computed Tomography (CT), Magnetic Resonance Imaging (MRI), Positron Emission Tomography (PET), functional MRI and Magneto-Encephalography. But above all these imaging modalities, MRI is the most widely used, since it has many advantages over other imaging techniques. Firstly, it does not use any ionising radiation. Secondly, it can generate, two-dimensional sectional images in any orientation, three-dimensional volumetric images or even four-dimensional images representing spatial-spectral distributions (Liang and Lauterbur, 2000). Lastly, the most important advantage of MRI over the other techniques is its high spatial resolution and contrast resolution (Wells *et al.*, 1996).

Therefore, for analysis purpose of this thesis, only MRI brain images were used.

1.2 AIMS

The aim of this thesis was performing qualitative and quantitative comparison of different segmentation algorithms by observing the performance of those algorithms in segmenting MRI brain images.

To achieve this, various segmentation techniques have been reviewed, after which, those algorithms which were used for actual comparison, were written and implemented in MATLAB®. Lastly, all developed algorithms were tested with brain MRI images and results were used for qualitative and quantitative comparison.

1.3 THESIS ORGANISATION

Chapter 2 reviews basic principles of MRI along with its parameters and artifacts.

Chapter 3 very briefly discusses topic of MR Image pre-processing specifically for brain images preprocessing.

Chapter 4 reviews MR image segmentation techniques. Firstly, it covers basic segmentation techniques like thresholding, region growing and edge-based segmentation. After introducing Fuzzy logic concept, it covers Fuzzy C-Means (FCM) segmentation algorithm, extensions of FCM and Improved Fuzzy C-Means (IFCM) algorithm.

Chapter 5 give details of source, type and parameters of data used for the practical implementation of this thesis.

Chapter 6 presents results and comparisons of different segmentation algorithm.

Chapter 7 presents final conclusions and future work possibilities.

CHAPTER 2

MAGNETIC RESONANCE IMAGING

2.1 HISTORY OF MRI

Magnetic Resonance Imaging (MRI) is a technique widely used in medical settings for diagnosis of many diseases. It produces high quality images of the inside of the human body. MRI is non-invasive because it does not use any ionising radiation and its particular advantage is high soft-tissue resolution. It is based on principles of Nuclear Magnetic Resonance (NMR); where NMR can be described as a spectroscopic technique used to obtain microscopic chemical and physical information about molecules (Hornak, 2007). The technique is called MRI instead of NMR; since the term 'N' was removed due to its associated negative connotations in 1970.

Felix Bloch and Edward Purcell independently discovered the magnetic resonance phenomenon in 1946 (Ellard, 2007). They were awarded the Nobel Prize in physics in 1952. In the late 60's and early 70's Raymond Damadian, demonstrated that the NMR tissue parameter (relaxation time T_1) of tumours differed to that of normal tissues (Ellard, 2007). This discovery gave a huge impetus to use Magnetic Resonance (MR) for the detection of disease. In 1973 Paul Lauterbur demonstrated use of MRI on small test tube samples (Hornak, 2007). He proposed the use of magnetic field gradients to differentiate the NMR signals coming from different locations. In 1975, Richard Ernst developed a two-dimensional Fourier technique for MRI. Over the last twenty years, Fourier transform imaging techniques have tremendously accelerated the development of MRI (Kumar *et al*., 1978). In 1977, Raymond Damadian proposed MRI termed as, field-focussing nuclear magnetic resonance. In the same year Peter Mansfield introduced echo-planar imaging (Hornak, 2007); while Hinshaw, Paul Bottomley, and Neil Holland, produced an image of the wrist (EMRF Foundation, 2007). Again in 1977, Damadian and colleagues succeeded in obtaining a cross section of a human chest. In 1978, Hugh

Clow and Ian R. Young reported the first transverse NMR image through a human head. In 1980, William Moore and colleagues obtained the first coronal and sagittal image through the human head (EMRF Foundation, 2007).

Looking at its brief history, MRI may be classified as a young science. But after coming through all these phases it is now undoubtedly a very developed technique and also superior to other imaging modalities such as x-rays, computed tomography and ultrasound.

2.2 BASIC PRINCIPLES OF MRI

2.2.1 Introduction

Magnetic resonance imaging is an exciting diagnostic imaging technique. It uses external magnetic fields and low-energy radio frequency (RF) signals to produce highly detailed images of the human body from specific atomic nuclei within the body (Geuns *et al.*, 1999). MR does not use ionising radiation to obtain images.

To understand MRI, it is essential to understand atomic behaviour. A single atom consists of a centrally-located nucleus and revolving electrons. The nucleus consists of protons and neutrons. Protons are positively charged, neutrons possess no charge, and electrons are negatively charged. The number of protons in the nucleus is denoted by atomic number, which also determines the type of element the atoms constitute. The sum of the neutrons and protons in the nucleus is called the mass number. If the number of electrons in an atom equals the number of protons, then it is considered as a stable atom. Atoms with a deficit or excess number of electrons are called ions (Westbrook, 2002).

The description of what happens when tissue is subjected to a magnetic field is provided by quantum mechanics (Puddephat, 2002). Nuclei, which have odd numbers of protons and neutrons, display a property called spin, which can be described as magnetic spin quantum number in quantum mechanics. When a nucleus rotates around its own axis it is called spin (motion). Since atomic nuclei possess charge, the spinning motion (of nuclei) generates a magnetic moment in the direction of the spin axis (Figure 2.1). Magnetic moment strength depends on the type of nucleus. The hydrogen nuclei (H^1) have the strongest magnetic moment and, are available in high abundance in the human body (in fat and water, 70% of the body is

made up of water). As a result, the hydrogen nucleus is the most preferred nucleus for MRI procedures.
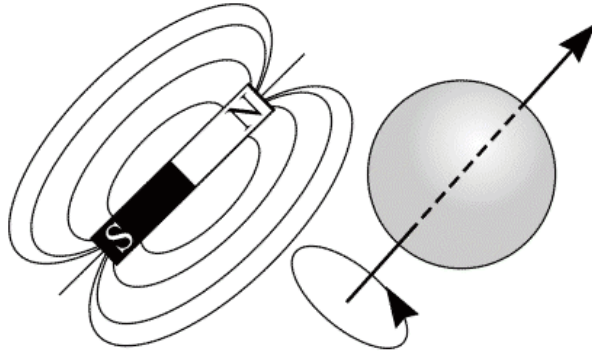
Figure 2.1 A charged, spinning nucleus creates a magnetic moment which acts like a bar magnet (dipole) (Puddephat, 2002).

Consider a group of H^1 nuclei (spinning protons) (Figure 2.2a). When no external magnetic field is present, the magnetic moments exhibit random orientations. When an external magnetic field B_0 is applied, the magnetic moments tend to align in the direction of the external magnetic field (Figure 2.2b).

(a)   (b)
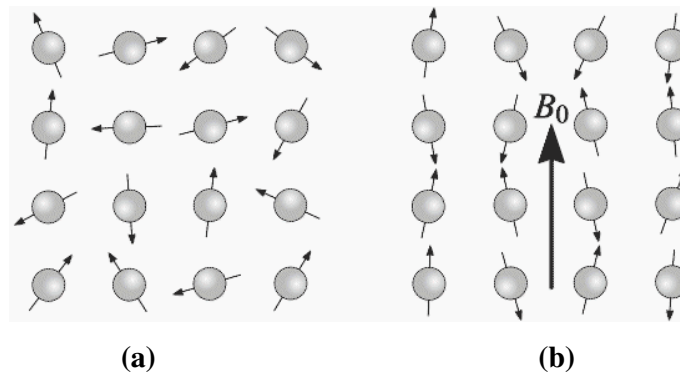
Figure 2.2(a) A collection of H^1 nuclei (spinning protons) in the absence of an externally applied magnetic field. The magnetic moments have random orientations. **(b)** An external magnetic field B_0 is applied which causes the nuclei to align themselves in one of two orientations with respect to B_0 (denoted parallel and anti-parallel) (Puddephat, 2002).

The magnetic moments or spins are bound to acquire either of the two orientations with respect to the external magnetic field B_0, termed as parallel or anti-parallel (Figure 2.3a). The angles between these orientations and B_0 are denoted as θ (Figure 2.3a). The spin axes are not exactly parallel with B_0; they precess with characteristic frequency around B_0 (Figure 2.3b). Nuclei with a similar magnetic spin quantum number show the same effects. Nuclei with higher magnetic spin quantum number possess more than two orientations.

(a)   **(b)**
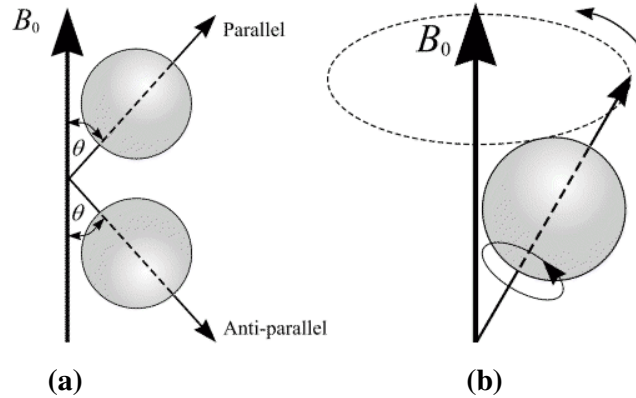
Figure 2.3 (a) In the presence of an externally applied magnetic field, B_0, nuclei is constrained to adopt one of two orientations with respect to B_0. As the nuclei possess spin, these orientations are not exactly at 0 and 180 degrees to B_0. **(b)** A magnetic moment precessing around B_0. Its path describes the surface of a cone (Puddephat, 2002).

An equation computing the relationship between the strength of magnetic field B_0, and the precessional frequency F of an individual spin is known as the Larmor equation. The Larmor equation is given as $\gamma B_0 = F$, where γ is called the gyromagnetic ratio of the nucleus and F is called the Larmor frequency. The gyromagnetic ratio for the hydrogen nucleus is 4257 Hz/Gauss (Mackiewich, 1995). Therefore, the precessional frequency of the hydrogen nucleus at 1.5 Tesla (T) is $F =$ 63.855 Megahertz (1T = 10,000 Gauss).

2.2.2 Radio Frequency field and MR Signal

Let us consider a group of H^1 nuclei. In this group, P_1 is the number of parallel spins and P_2 is the number of anti-parallel spins with corresponding energy levels E_1 and E_2, respectively. Energy level E_2 of the anti-parallel spin is always greater than energy level E_1 of the parallel spin, and consequently P_1 is greater than P_2. If the exact amount of energy difference $E_2 - E_1 = \delta(E)$ between these two states is applied to the system, then spins P_2 moves to P_1. For a 1.5 Tesla magnetic field at room temperature, the population ratio of P_2: P_1 will be 100,000: 100,006 (Puddephat, 2002).

Magnetic moments of group H^1 nuclei can be represented as vectors (Figure 2.4). Every vector can be divided into two components; one perpendicular and the other parallel to B_0. If we consider a cone of spins as in the accompanying figure, then components in the perpendicular direction to B_0 cancel out with each other, and consequently components in the direction parallel to B_0 produce the result. The net magnetisation (vector) is in the direction of B_0, because parallel spins outnumber anti-parallel spins.
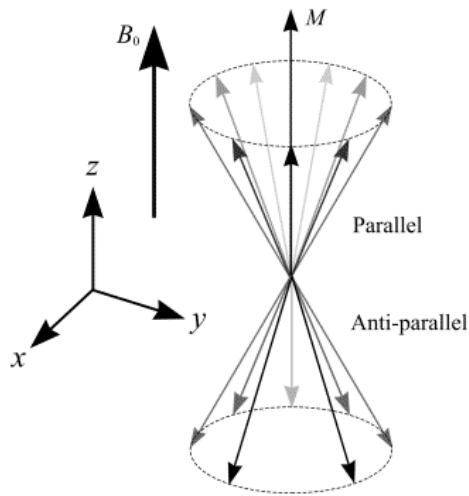
Figure 2.4 A collection of spins at any given instant in an external magnetic field, B_0. A small net magnetisation, M, is detectable in the direction of B_0 (Puddephat, 2002).

Let us consider that B_0 is parallel in the direction with x-axis of Euclidean 3-space (Figure 2.5); then the plane perpendicular to B_0 will have x- and y-axes of Euclidean space. If we apply an energy equal to the difference between two spin states, then we can obtain a signal from the H^1 nuclei. This can be achieved by applying radio frequency (energy) at the Larmor frequency, which leads to the swapping between parallel and anti-parallel spin states. The swapping of spin states creates wobble on the component of M parallel to the z-axis. Radio frequency energy consists of two components, namely the magnetic field component and the electric field component. If we denote the magnetic field component that lies in the x-y plane as B_1 (Figure 2.5), then B_1 combines the x-y components of M to eventually change the direction of M into the x-y plane from the z-plane.

Change in the angle of M from the z-axis is known as the flip angle. Conversion of spins between parallel and anti-parallel states depends on the strength and period of B_1. If we apply pulses of 90° and 270° then, because of the total shift of the z-component of M, the population of spins states P_1 and P_2 becomes exactly equal. A radio frequency pulse of 180^0 tilts M into exactly opposite with B_0, while longer application of field B_1 rotates M from the z-axis to the x-y plane, again returning to the z-axis (original position).
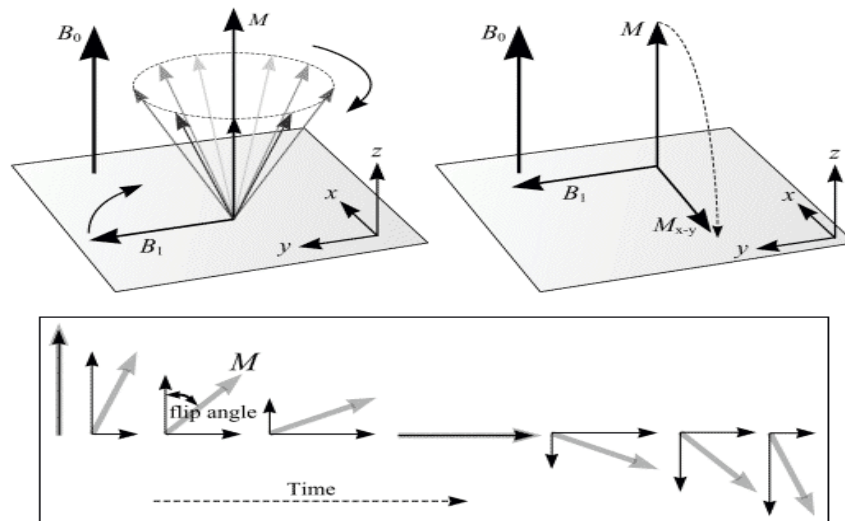
Figure 2.5 (Top) The effect of RF radiation on the net magnetisation vector M is to produce a second magnetic field Mx-y. M is tilted from its original longitudinal z-axis orientation, along the direction of the external magnetic field B_0, into the transverse

x-y plane. **(Bottom)** An illustration of flip angle, which is the angle through which *M* has rotated away from the *z*-axis (Puddephat, 2002).

As discussed above, the radio frequency (RF) pulse causes *M* to flip in the *x-y* plane and rotate around B_0. This precession of *M* around the B_0 axis induces an electromotive force in the receiver coil (placed in the vicinity). The magnetic resonance image is obtained from the signal received by the receiver coil. The plot known as free induction decay (FID) is a plot of signal received in the receiver coil with respect to time.

(a)   (b)
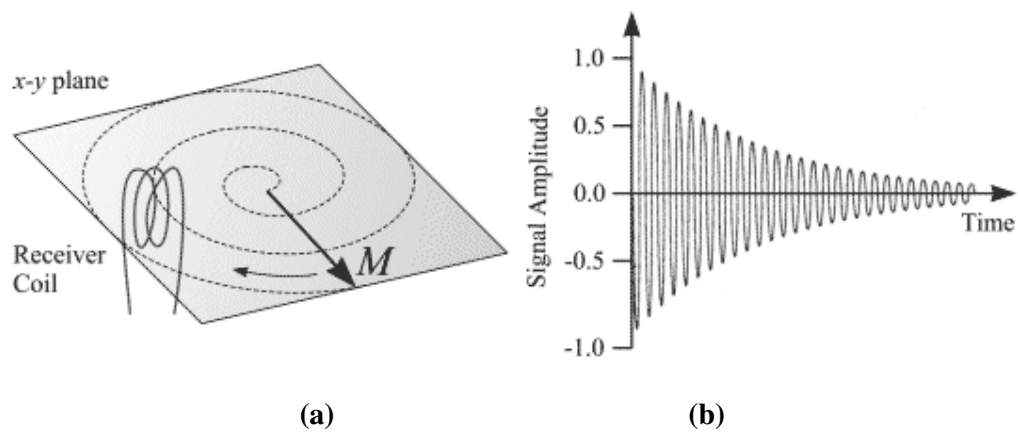
Figure 2.6(a)   After a 90 degrees RF pulse, *M* lies in the *x-y* plane and rotates about the *z*-axis. The component of *M* in the *x-y* plane decays over time.
(b) An alternating current induced in the receiver coil (Puddephat, 2002).

2.2.3 Relaxation Processes
When *M* returns to its original position parallel to the *z*-axis, it is called the relaxation process. Two types of relaxation process exist, widely known as longitudinal T_1 relaxation (or spin lattice) and transverse T_2 relaxation (or spin-spin relaxation). T_1 relaxation and T_2 relaxation processes are discussed in detail along with other parameters in the following MRI parameters section.

2.2.4 Magnetic Resonance Imaging

Magnetic field gradients are used to locate the exact location of nuclei emitting the RF signal. Generally, magnetic field gradients are created by situating two coils of wire (opposite in direction) surrounding the main magnetic field B_0 and passing direct current through the coils. Gradient magnetic field sums up with B_0, creating two ends of different magnetic field strength higher and lower. Because of a magnetic field gradient, identical nuclei precess at different Larmor frequencies and a difference in the frequency depends on the distance between nuclei and gradient coil centre and current flowing through the coil.

2.2.4.a Slice Selection

Due to magnetic field gradient, it is possible to select a slice from the region which image is desired. Applying a single RF pulse, due to which only the selected plane perpendicular to the longitudinal axis absorbs the RF frequency, can enable this slice selection.

2.2.4.b Frequency Encoding

To obtain a detailed imaging of any part of the subject under study, three gradient magnets arranged in orthogonal positions are used. One gradient magnet is used for slice selection as discussed above, while one of two other gradient magnets can be used for frequency encoding. When the second gradient coil is excited, it does spatial encoding of the selected slice along one axis, while spin columns perpendicular to the selected slice precess at a different frequency.

2.2.4.c Phase Encoding

When slice selection and frequency encoding is done as discussed above, then after short period of time the phase of spins at one end of gradient magnet runs ahead of the phase of spins at other end. This happens because spins at one end of the gradient magnet precess faster than at the other end. After frequency-encoding gradient is switched of the phase difference at two ends continues to remain, and this is called as phase memory. The phase encoding gradient is applied after slice selection and excitation but before frequency encoding.

2.2.4.d Image Formation

If a 256x256 pixel image has to be formed, then the pulse sequence is executed 256 times and the phase encoding gradient is changed for all these iterations. When this process is carried out, field strength decreases step by step to zero, and then increases again up to its original value but in the opposite direction. As mentioned above, for a 256x256 image size, when scan completes it produces 256 lines each corresponding to 256 samples of frequency. Each pixel in the image can be defined with the help of Fourier transformation that assigns correct phase and frequency corresponding to the appropriate volume element. Gray scale image can be constructed from intensity information. The basic principles of MRI have been described (Puddephat, 2002) and the brief details of MRI sequences (Westbrook and Kaut, 1994) are described in the next section.

2.3 MRI PARAMETERS

Signal intensity of MRI depends mainly on proton density, and T_1 and T_2 relaxation times. The time between two consecutive RF pulses is called the repetition time (TR). TR decides the amount of T_1 relaxation. The longer TR gives more time for recovery of longitudinal magnetisation. Tissues with shorter T_1 have stronger signal intensity than tissues, which possess longer T_1. Longer TR allows more recovery of magnetisation, which results in less difference between T_1 contributions. Echo time (TE) is the time from the application RF pulse to measurement of that signal. TE is the factor, which decides when the signal is to be measured or how much transverse magnetisation decay is allowed before measurement of signal. TE determines the amount of T_2 relaxation. MR image contrast can be controlled with the help of variation in TR for RF pulses and with variation in TE for received signals.

Commonly used MRI images are, T_1-weighted, T_2-weighted, and proton density (PD) weighted. If in an image, contrast is predominated by T_1 signals then it is called a T_1-weighted image. To obtain this type of image, TR is kept short to exaggerate T_1 and TE is kept short to decrease T_2. Similarly, when an image contrast is predominated by T_2 signals it is called a T_2-weighted image. To obtain T_2-weighted image long TE and long TR are used, which exaggerates T_2 and diminishes T_1, respectively. Proton density image mainly depends on the density of protons by

decreasing the effects of T_1 and T_2. Therefore longer TR and shorter TE are used to decrease both T_1 and T_2 (Fonar Corporation, 2003).

In T_1-weighted images, tissues which possess short T_1 recovery times, produce a high signal and as a result appears bright e.g. fat. Since these types of tissues are able to recover maximum magnetisation during TR, when the next RF pulse arrives, more magnetisation is available to allow them to be flipped into the transverse plane. Tissues which have long T_2 decay times, appear bright e.g. water. Since they are able to retain their maximum transverse coherence during the TE period. In PD weighted images, tissues having a high number of protons appear bright, e.g. cortical bone. Since large numbers of protons in that area cause large transverse magnetisation component.

Appearance of some typical tissues in different types of MR images is shown in Table 2.1 below.

Table 2.1: Typical tissue's brightness in different MR images (Hesselink, 2003)

Tissue	T_1-weighted	T_2-weighted	PD-weighted
Fat	Bright	Dark	Bright
Cyst	Dark	Bright	Grey
White matter	Bright	Grey	Grey
Gray matter	Grey	Bright	Bright
CSF	Dark	Bright	Grey

2.4 MRI PULSE SEQUENCES

A specific set of RF pulses applied in order to produce a specific form of MR image is termed as pulse sequence. Signals are determined by variable parameters based on pulse sequences used (Hornak, 2007).

Below are some commonly used pulse sequences in MRI (Ballinger, 1996).

- Inversion recovery sequence
- Gradient echo sequence
- Diffusion pulse sequence
- Saturation recovery sequence
- Echo-planar sequence
- Spiral Pulse sequence.

2.5 MRI ARTIFACTS

Though MRI artifacts do not come into direct scope of this thesis, reason of their inclusion in this section is that they make intensity-based segmentation methods difficult. Therefore for the study of segmentation, familiarity with common image artifacts is useful. Also, MRI images with artifacts are used in further sections for practical implementation of this thesis.

An image artifact is any feature, which appears in an image and which is not present in the original imaged object (Hornak, 2007). Image artifacts result in an image that does not portray (in the simple visual sense) an accurate representation of a slice of tissue (Savoy and Jovicih, 2001). Artifacts can arise as a result of improper imaging or can be a consequence of natural processes or properties of the human body itself. It is important to familiarise oneself with the appearance of artifacts, because they can significantly affect the quality of MR images and may be mistaken with pathology, causing incorrect diagnosis. Artifacts are typically classified on the basis of their sources. They can be stated as flow, motion, RF noise, RF inhomogeneity, gradient, partial volume, gibbs ringing, etc. Below are the most common artfifacts encountered in MRI (Ballinger, 1996).

Chemical Shift Artifact:

The chemical shift artifact is commonly noticed in the spine at the vertebral body end plates, in the abdomen, and in the orbits where fat and other tissues form borders. It is caused by difference in chemical environment (Larmor frequency) of fat and water. In fact fat and water are both made up of hydrogen protons, fat consists of hydrogen linked to water but water consist of hydrogen linked with oxygen. Because of this structure, resonance frequency of hydrogen in fat is lower than that of water. As a result of difference in resonant larmor frequency, frequency shift inherently occurs between fat and water, known as chemical shift. Magnitude of chemical artifact depends on the magnetic strength; a low magnetic strength for imaging can reduce this type of artifact. In Figure 2.7, the arrows points out the exact location of chemical artifact.

Figure 2.7   **Figure 2.8**

Figure 2.7 In this case study (image) the chemical shift artifact is visible (arrow pointed) as a small dark or bright border at the interfaces of bone, fat and muscle, best seen in the upper part of the head (MR technology information portal, 2007).

Figure 2.8 The accompanying sagittal image of the head contains an RF inhomogeneity artifact in the region of the mouth (see arrow). The patient has a large amount of non ferromagnetic metal dental work in the mouth; the metal shielded the regions near the mouth from RF pulses thus producing a signal void (Hornak, 2007).

RF Inhomogeneity Artifact:

RF inhomogeneity artifact is the result of unwanted intensity variation across an image. This intensity variation is caused by nonuniform external magnetic field or by variable sensitivity in an RF coil. Some RF coils, such as surface coils, naturally have variations in sensitivity and will always display this artifact. The presence of this artifact in other coils represents the failure of an element in the RF coil or the presence non-ferromagnetic material in the imaged object. As this artifact depends on magnet and RF coils, proper selection of them may result in reduction of this artifact. Superconductive magnets are the most commonly used magnets, which can maintain a homogenous field over time (Aziz and Uetani, 2002; Douglas, 1998). Figure 2.8 shows the sagittal image of the head containing an RF inhomogeneity artifact in the region of the mouth.

Motion artifact:

Motion artifacts are caused by motion of the patient or motion of part of patient. The patient motion during the imaging sequence generally results in a blurring of the complete image with ghost images in the phase encoding direction. Movement of a part of a patient results in a blurring of that particular part in the image. Prevention of the voluntary motion of the patients is possible up to much extent, but elimination of involuntary motion such as heart beating, breathing, bowel motion etc is not possible. Heart beating and breathing motion can be minimised by gating the imaging sequence to the cardiac or respiratory cycle of the patient. Bowel motion can be reduced by giving the patient an anti-spasmodic agent prior to the scan when imaging the abdomen or pelvis (Westbrook and Kaut, 2002b; Aziz and Uteani, 2002). Figure 2.9 shows motion artifact in a head axial image. A blood vessel in the posterior side of the head moved in a pulsating motion during the acquisition. This motion caused a ghosting across the image.

| **Figure 2.9** | **Figure 2.10** |

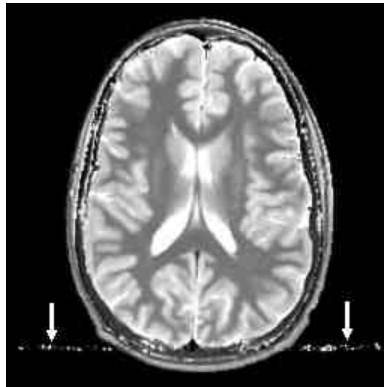**Figure 2.9** The arrow shows the ghosting across the image because of pulsating motion of blood vessel (in the posterior side) during image acquisition (Hornak, 2007).

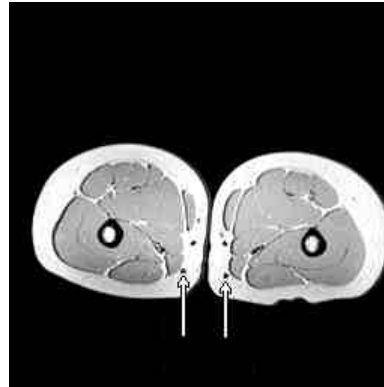**Figure 2.10** The arrow shows the position of the blood vessels which appear black even though they contain a large amount of water, since by the time signal was recorded liquid (water) has moved out of the place resulting in black spots (Hornak, 2007).

Flow Artifact:

Blood flow or flow of liquid in the body while imaging the patient is cause of flow artifact. In flow artifact it may happen that, a liquid flowing through a slice (selected for imaging) will experience an RF pulse and by the time the signal is recorded liquid flows out of the place. This can result in different signal intensities of blood vessels. For example, the intensity of a vessel perpendicular to the image plane changes periodically due to pulsatile blood flow (Douglas, 1998; Siemens, 2001). Figure 2.10 shows an axial slice through the legs. In slice blood vessels appear black because of flow artifact even though they contain a large amount of water.

Aliasing or Wrap Around artifact:

This is a usual artifact produced when the field of view (FOV) is smaller than the size of the anatomy being imaged. The FOV is the physical size of the imaged region (Siemens, 2001). In this artifact (as FOV is smaller), objects located outside the FOV appear at the opposite side of the image, as if one took the image and wrapped around a cylinder. The primary solution to this artifact is oversampling, which is the digitisation of a time domain signal at a frequency much greater than necessary to record the desired FOV (Aziz and Uetani, 2002). Figure 2.11 shows the sagittal image of the head, in which nose appears at the back of head.
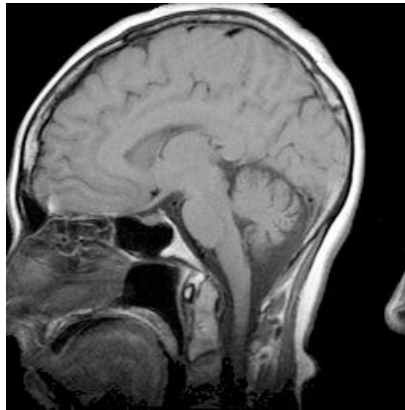

Figure 2.11

Aliasing artifact (Hornak, 2007).

Truncation or Gibbs Artifact:

Truncation artifacts are caused by incomplete digitisation or in other words from under sampling of data; as a result interfaces of high and low signal are incorrectly represented on the image. This artifact produces a series of bright and dark lines parallel to a sharp intensity edge in an image. This artifact is commonly seen in the T_2 –weighted image, where there is bright CSF next to dark spinal cord. It is also seen in other locations such as brain and calvarium interface. To reduce this artifact, under sampling should be avoided (Westbrook and Kaut, 20002b; Ballinger, 1996). In Figure 2.12 the fine lines visible in the image on the left are due to undersampling of the high spatial frequencies. This results in a "ringing" type of artifact following these borders in the phase direction (R to L in this image). This problem can be easily fixed by taking more samples such as the image on the right with 256 phase encodes.
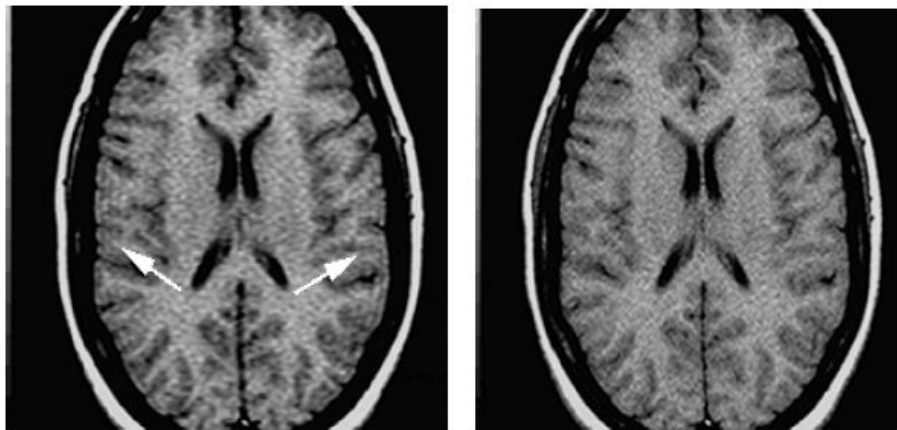
Figure 2.12

Truncation or Gibbs ringing artifact (Ruan, 2003).

Partial Volume Artifact:

A partial volume artifact is any artifact, which is caused when the size of the image voxel (the smallest discrete spatial component of the image) is larger than the feature to be imaged. For example, a small voxel may contain a signal from one tissue type (i.e. fat/ water), and a larger voxel may contain a combination of two types, whose signal intensity is equal to the weighted average of the quantity of two tissues in the voxel. It may manifest as a loss of resolution caused by multiple features present in

the image voxel (Douglas, 1998). Use of smaller voxel may minimise this artifact but, this may lead to poorer signal to noise ratios in the image.

Accompanying figure 2.13 shows a comparison of two axial slices of the head taken through same location of the head. One image is taken with 3mm slice thickness while the other with 10mm slice thickness. There is apparent loss in resolution and in 10mm slice thickness image.

(a)   **(b)**

Figure 2.13(a) 3mm slice thickness. **(b)** 10mm slice thickness; There is an apparent difference in resolution of two images/slices (a and b) through the same location, because of partial volume artifact. 10mm slice thickness produces poor image resolution as compared to 3mm slice thickness image. Loss of details can be easily seen in 10mm slice thickness image (Hornak, 2007).

CHAPTER 3
MR IMAGE PREPROCESSING

Since MR image segmentation is of importance to this thesis therefore MR image pre-processing is not in direct scope of it. But as pre-processing of t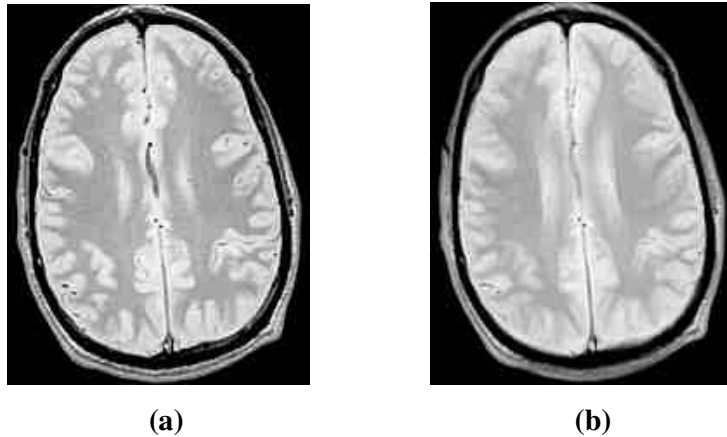he MR images is preliminary and necessary initial step for carrying out effective segmentation, it is discussed very briefly here. MR image pre-processing for brain images can be typically categorised into the following three steps (Shen *et al.*, 2003).

1. Image Standardisation: A major problem with MRI is that, even in the same body region of the same scanner signal intensities do not have a fixed value (Nyul and Udupa, 1999). As a result of this, similar type of tissue may possess different scales of signal intensity in the different images. Therefore in order to bring uniformity in the signal intensities of different tissues, image standardisation is carried out.

2. Non-Brain Region Removal: This can be a part of MR image pre-processing if only brain region is of particular interest. If non-brain region is out of interest and if it is not removed in pre-processing then, it may greatly affect segmentation results.

3. Tissue Contrast Enhancement: This may be part of MR image pre-processing particularly when there is a requirement of enhancing tissue contrast between white matter and gray matter.

As mentioned above image pre-processing was out of scope of this project. But out of the three step image pre-processing method mentioned above only image standardisation was used for practical implementation of this thesis; as standardisation of image is an imperative process before performing image segmentation. For carrying out standardisation of images algorithm was written and developed in MATLAB$^{®}$ and (results) standardised images were used for segmentation. Standardisation algorithm developed for this thesis was based on the

method proposed by Shan Shen (Shen, 2004). This method maintains basic intensity features of the images and standardizes the intensity. The method uses statistical analysis, in which statistical features of the pixel intensities are considered for the statistical analysis.

CHAPTER 4

MR IMAGE SEGMENTATION

4.1 INTRODUCTION

Image segmentation is a procedure that spatially partitions an image into a certain number of homogeneous regions or isolates specific objects in an image (Robb, 2000; Kurz and Benteftifa, 1997). Classification of homogenous regions or isolation of specific objects depends on some criteria such as grey level, colour and texture.

Image segmentation is a vital part of image processing, and the technique has proven to be useful in numerous fields, due to its characteristic of extracting required and useful information. In photography it is used in face recognition and aerial photography recognition, to identify face and objects respectively by extracting useful information. In medicine, it is used to distinguish different tissues so that a specific measurement can be done automatically (Li and Gray, 2000). In industrial applications segmentation is used to differentiate appropriate components for assembly systems.

A number of segmentation techniques have been proposed over the years, including thresholding, region growing, edge-based segmentation and clustering. Each technique has its own advantages and flaws.

4.1.1 Thresholding

Thresholding can be said to be one of the basic segmentation techniques. Initially, a threshold is chosen based on the image histogram or co-occurrence matrix (Pal and Pal, 1993) to separate the image into two sub-regions. After separation of the image into two sub-regions each region is assigned its own threshold, therefore there will be two thresholds if there are two sub regions after first iteration. This way a new threshold is calculated iteratively for each sub region. More accurate the threshold level(s) better the result of image segmentation. In a few cases it is very easy to assign threshold values to the regions because of their obvious difference in gray level. But in most cases of a medical/clinical context, images are fairly complex and

threshold determination becomes a very difficult task. Cheriot *et al.* (1998) devised a thresholding technique, based on division of pixels into background and region of interest. In this technique, division (of pixels) is based on the image histogram and each time the largest peak is removed (from gray level histogram) until there are no peaks left. Though this method tries to improvise segmentation technique, real problem occurs in case of unimodal histogram (histogram having only one peak). Unimodal histograms are quiet common in medical images and they appear mainly because of the large number of background pixels.

Thresholding is being used for MR image segmentation in a number of ways throughout the years and through out the world. Suzuki *et al.* (1991) tried to segment brain tissues in axial MR slices with the help of repetitive thresholding. New thresholds were iteratively updated from the geometry of the resulting mask. Lemieux *et al.* (1999) used a method of automatic thresholding along with morphological operations to develop a three-dimensional technique. The technique uses the whole image histogram for choice of thresholds, and after that uses morphological operators to separate the segmented image. Determination of threshold levels from whole image histogram alone does not prove to be a very good technique because of complex distribution of tissue intensities in the brain image.

Lee *et al.* (1998) proposed an unsupervised connectivity based thresholding segmentation of mid-sagittal brain MRI images. They used thresholding to obtain binary images; from binary images they obtained some landmark tissues. Based on these landmarks and anatomical information they processed binary images, which substantially simplify the subsequent operations. Recently, Taheri *et al.* (2007) devised a thresholding algorithm for three dimensional tumour segmentation. This algorithm performs global thresholding to form so called level set speed function. This function is updated iteratively throughout the level set growing process. Important feature of this level set method is no explicit knowledge about tumour and non tumour density functions is needed.

4.1.2 Region Growing

Region growing is an up-grading of thresholding. The connectivity condition (four or eight connected pixels) is combined with thresholding to perform the segmentation

(Robb, 2000). To perform a segmentation using a region growing technique, one must know the number of regions to be segmented and location of one pixel or several pixels for each region. These initial pixels are known as seeds or seed pixels and they are determined manually or using computer based methods. Based on these seeds region grows by grouping each pixel in suitable region depending on thresholding and connectivity criterion. The process of region growing does not stop until there is no connected pixel left satisfying the thresholding criterion. As region growing technique works relying on seeds, it is very obvious that its accuracy and precision depends on correct selection of seeds. If seeds are properly chosen the obvious result is better segmentation and if choice of seeds is improper then segmentation results can be really poor and inaccurate. There are some ways to decide the seeds but generally they are brightest pixels from the region or they can be determined by looking at peaks in histogram. As region growing uses connectivity criteria along with thresholding, it has more accuracy as compared to thresholding. But it is certainly time-consuming method than simple thresholding because of its longer computational times. Also segmentation methods in region growing category are all sensitive to the initial seeds (Gonzalez and Wintz, 1977).

To use region growing as efficient segmentation technique for medical images, there is a necessity of precise anatomical information. Since based on this information proper choice of seeds for each region and the region homogeneity is possible. Pohle and Toennies (2001) put forward a region-growing algorithm, which was based on model of regions and their homogeneity. Their algorithm was based on the assumption that gray level deviations are less within one region as compared to between regions and these gray levels will follow certain homogeneity criterion. The problem with this technique arises in case of noisy conditions since in those cases region homogeneity criterion cannot work properly. Law and Heng (2000) presented a technique, which was working by repetitively incrementing the deviation of the regions in the search of optimal thresholds. This increment in deviation will continue until the number of pixels in the regions suddenly increases and thus regions are separated. So many region-growing methods were put forward but all has certain flaws.

4.1.3 Edge Based Segmentation

Edge based segmentation has a large group of methods of segmentation based on edges of the image. Edge based segmentation generally extract the edge by discovery of grey level discontinuity in the image. Extraction of grey level discontinuity in the image is preliminary process in edge-based segmentation and this is done with edge detecting operators, such as Roberts, Prewitt, Sobel and Laplacian. Edge based segmentation alone is not used as segmentation technique, generally there are some methods followed by edge segmentation to combine edges into edge chains. Depending on closeness of these chains they can become the borders in the image. If the regions are clearly defined by these borders then segmentation can be done to separate the image into regions. Most common problem of many edge based segmentation techniques can be said as presence of an edge in place where there is no border and no edge where a border exists (Zhang, 1997). This improper edge classification is result of image noise and or unsuitable information in image.

Edge based segmentation is fairly old technique and number of methods have been proposed through out the years. Gibbs *et al*. (1996) proposed a method to perform MR image segmentation in which they used morphological edge detection and region growing together. Lin, Tian and He (2002) developed a method of segmentation using fuzzy object extraction and edge detection, which they applied on MR images. Many methods proposed were combination of edge-based segmentation and other methods, but still they cannot be called as flaw less and very effective.

Edge detection is purposely used in this thesis as one of the segmentation techniques for performing comparisons between different segmentation techniques. Use of edge detection technique will show how classical and basic segmentation technique such as edge detection performs in comparison with advanced techniques like fuzzy clustering. Above-mentioned Roberts, Prewitt and Sobel operators are used for detecting edges and segmenting images.

4.1.4 Clustering

Clustering can be said to posses some advantages compared to previously discussed techniques, because of its unsupervised nature. Clustering does not require any initial

information or training data like seeds in edge-based segmentation. Cluster means group of pixels having similar features and in clustering, image is partitioned into similar groups called as clusters. Cluster feature is meant by grey level value and therefore separation of pixels into clusters having similar features means separation of pixels into clusters or groups having similar grey level values. In this way pixels belonging to one cluster will have similar grey level values while pixels from two different clusters will have different grey level values. In general clustering methods are categorised into three types, deterministic, fuzzy and statistical methods. Each type above has its representative algorithm k- means clustering, fuzzy c-means (FCM) clustering, and expectation maximization (EM) algorithm respectively (Cannon *et al.*, 1986).

The K-means technique involves iterative computations for computation of grey-level centre for each cluster. Differentiating each pixel into the cluster with closest centre performs the K-means segmentation process. The algorithm based on fuzzy set theory and therefore which is fuzzy equivalent of K-means clustering algorithm is FCM. It takes into account the overlapping of the clusters and allows partial belongingness of the pixels to all the clusters (Kettaf et al., 1996). Because of these properties FCM algorithm is better in cases of segmentation of images with uncertainty like medical images. EM algorithm is based on assumption that data follows a Gaussian mixture model. It considers the clusters as missing information and computes the maximum likelihood estimates of the mean, covariance, and mixing coefficients of the mixture model (Coleman and Andrews, 1979; Powers, 2000).

Clustering is the most widely used segmentation technique for medical images, and more so in case of FCM and EM. Wells *et al.* (1996) introduced a new method called adaptive segmentation. Adaptive segmentation was used for segmentation of brain images. It uses EM on intensity inhomogeneity of different tissues for segmentation. Leemput *et al.* (1999) put an automated model based segmentation method forward. They introduced automated model based segmentation method based on EM technique. In this method tissue classification is done by estimation of tissue-class-specific intensity models. But this segmentation method was also not efficient because of common flaw of EM that is, intensity

distribution of brain images is regarded as normal distribution, which is not true for medical images with uncertainty or noise. Because of this disadvantage, EM method has limitations. Many researchers tried to use FCM algorithm for brain image segmentation. Li *et al*. (1993) presented FCM for brain image segmentation. They used knowledge based classification and tissue labelling approach for segmentation. After that the same researchers introduced an expert system to locate a landmark tissue by matching it with prior model. Hall *et al*. (1992) did the comparison of FCM and neural networks in segmenting brain MR images. They concluded FCM performs better segmentation on normal brains but performs very badly on abnormal brains with oedema and tumour. Pham and Prince (1999) tried to improve traditional FCM algorithm for dealing with MR images corrupted by intensity inhomogeneities. FCM seems to perform better than basic methods in case of medical image segmentation but its major flaw is sensitivity to noise. Sensitivity to noise is also shortcoming of many intensity based segmentation methods.

In recent developments in clustering, Greenspan *et al.* (2006) proposed an automated segmentation algorithm for noisy and low contrast brain MRI images. They used Gaussian mixture model and EM algorithm for carrying out this automated segmentation. Selvathi *et al.* (2005) devised a combination of FCM and genetic algorithm for an automatic segmentation of white matter, gray matter, cerebro spinal fluid the extra cranial regions and presence of tumour regions. Li *et al.* (2006) put forward a new FCM clustering algorithm based on technique called as particle swam optimisation; authors mention that this new algorithm is more robust and performs effective segmentation than pure FCM.

4.2 *K*-MEANS CLUSTERING ALGORITHM

Mac-Queen (1967) first proposed the *K*-means algorithm. *K*-means is one of the simplest unsupervised algorithms based on the clustering technique. It works with simple technique for classification of a given set of data into number of *K* clusters. It works by minimising an objective function *J*

$$J = \sum_{j=1}^{k} \sum_{i=1}^{n} \left[d^2 \cdot \left[\left(X^j \right)_i - C_j \right] \right] \tag{4.1}$$

where difference between function (X^j_i) and C_j is a distance measure between a data point (X^j_i) and the cluster centre C_j, this distance is a representation of the distance of the n data points from their respective cluster centres.

The algorithm works with following steps:

(1) Initiate the number of clusters K; these also represent the initial centroids.

(2) Assign each pixel to the cluster, which has closest value of centroid.

(3) When all pixels are assigned to particular clusters then recalculate the positions of K centroids.

(4) Repeat Procedures 2 and 3 until the centroids no longer move.

4.3 FUZZY LOGIC

4.3.1 Introduction

To understand fuzzy-based segmentation algorithms, a basic knowledge of fuzzy logic is necessary. This section introduces the concept of fuzzy logic.

Zadeh first conceived the concept of fuzzy logic in 1965 (Zadeh, 1965) at the University of California in Berkeley. In 1974 Mamdani and Assilain used a fuzzy logic technique to regulate a steam engine. At this point fuzzy logic received some attention. In 1985 researchers at Bell laboratories developed the first fuzzy logic chip. In 1993, OMRON developed the first fuzzy computer (Dutta, 1993). Nowadays, fuzzy logic has become one of the fastest growing techniques of applied artificial intelligence technology (Stelzer, 2003).

Classic logic, which is based on Boolean logic, assumes that every fact is either entirely true or false (can never be both). Unavoidable and inherent restriction of this technique is its incapability in representing incomplete and imprecise information.

Taking an example, Boolean logic is used to categorise whether a train is 'fast' or 'slow'. If the given threshold is 100 miles/hr, trains running with this speed or higher are considered as 'fast', otherwise 'slow'. According to this threshold, if the train's speed is 99.9miles/hr or 95miles/hr it will be considered as 'slow'; but 0.1mile/hr or even 5mile/hr is too small to be considered.

Fuzzy logic takes Boolean logic one-step further to deal with this type of problem, by creating a provision of assigning intermediate values. Fuzzy logic uses a

membership function, which describes the degree of truth with real values between zero and one (inclusive). If value of membership function is zero it indicates completely untrue and if value is one it signifies hundred percent true (unlike the classic logic). All values between the two (zero and one) indicate partial membership to the truth. Looking once again at the previous example, if we use fuzzy logic to represent the speed of the train, a speed of 100miles/hr would have membership value of one while 60miles/hr would have membership value of zero. Therefore if a train is running with the speed of 99miles/hr it would have membership value close to one, like 0.97 or so and a speed of 63miles/m would have a membership value close to zero, like 0.1.

Boolean logic is also known as binary logic, and then fuzzy logic can be called as multi-valued logic. This logic allows intermediate values to be defined between convention evaluations like true/false, yes/know, high/low, etc. Notions like rather tall or very fast can be formulated mathematically and processed by computers, in order to apply more human like way of thinking in the programming of computers (Zadeh, 1965).

4.3.2 Membership Function

The membership function in fuzzy logic is a mathematic function, which is variable according to the particular problems. Taking into consideration the train example discussed above, speed can be presented as:

$$
\text{Membership} = \begin{cases} 0 & \text{speed} < 60\text{miles/hr} \\ ((\text{speed} - 100) / 40) & 60\text{miles/hr} \leq \text{speed} \leq 100\text{miles/hr} \\ 1 & \text{speed} > 100\text{miles/hr} \end{cases}
$$

Now consider one more example, which shows another type of membership. The example is of membership function of warmness. Suppose 45-75ºC is considered as warm, then temperatures below this range will be cold and over this range will be hot. Then the membership function will have a maximum value of one in the middle and will decrease on both sides. Membership functions can be represented as follows:

$$
\text{Membership} = \begin{cases}
0 & T < 0° \\
T/45 & 0°C \leq T \leq 45°C \\
1 & 45°C < T \leq 75°C \\
1- ((T-75)/75) & 45°C < T \leq 75°C \\
0 & T > 75°C
\end{cases}
$$

4.3.3 Applications

As mentioned previously fuzzy logic is a better technique to handle vague data and model imprecise reasoning procedures. Many commercial applications of fuzzy logic relate to control systems. Some of the practical applications of fuzzy logic are (Bauer, Nouak and winkler, 1996):

- Automatic control of dam gates for hydroelectric-power plants (Tokio Electric Pow)

- Camera aiming for the telecast of sporting events (Omron)

- Combination of fuzzy logic and neural nets (Matsushita)

- Cruise control for automobiles (Nissan, Subaru)

- Efficient and stable control of car- engines (Nissan)

- Flight aid for helicopters (Sugeno)

- Improved efficiency and optimised function of industrial control applications (Aptronics, Omron, Meiden, Sha, Micom, Mitsubhishi, Nisshin-Denki, Oku-Electronics)

- Improved fuel-consumption for automobiles (NOK, Nippon Denki Tools)

- Medicine technology: cancer diagnosis (Kawasaki Medical School)

- Recognition of motives in pictures with video cameras (Canon, Minolta)

- Simplified control of robots (Hirota, Fuji Electric, Toshiba, Omron)

Along with the applications described above, fuzzy logic is a very important technique in various segmentation methods. Fuzzy-based segmentation algorithms are described in the following sections.

4.4 FUZZY C-MEANS CLUSTERING ALGORITHM

The most commonly used FCM algorithm was proposed by Bezdek (Bezdek, 1981). Bezdek tried to improve earlier clustering methods. Before Bezdek Dunn developed

the FCM algorithm (Dunn, 1973). FCM is an iterative algorithm. It is based on minimization of an objective function, with respect to fuzzy membership U, and a set of cluster centroids V:

$$J_m \cdot (U,V) = \sum_{j=1}^{N} \sum_{i=1}^{C} \left[\left(u^m \right)_{ij} \cdot d^2 \cdot \left(X_j, V_i \right) \right] \tag{4.2}$$

In the above equation, $X = \{x_1, x_2, \ldots x_j, x_N\}$ is a $p \times N$ data matrix, where p stands for the dimensions of each x_i "feature" vector (grey level, colours etc in images), and N stands for the number of feature vectors (pixel numbers in images). C represents the number of clusters. $u_{ij} \subseteq U(p \times N \times C)$, is the membership function of vector x_j to the j-th cluster, which satisfies: $u_{ij} \in [0,1]$ and $\sum_{i=1}^{C} u_{ij} = 1$, ($j = 1, 2, \ldots N$). The higher membership indicates the higher the probability that the pixel belongs to the cluster. The membership function is given as follows:

$$u_{ij} = \frac{1}{\sum_{k=1}^{C} \left[\frac{d \cdot \left(X_j, V_i \right)}{d \cdot \left(X_j, V_k \right)} \right]^{\frac{2}{m-1}}} \tag{4.3}$$

$V = \{v_1, v_2, \ldots v_i \ldots v_c\}$, which is a $p \times C$ matrix, and represents the cluster feature centre:

$$V_i = \frac{\sum_{j=1}^{N} \left[\left(u_{ij} \right)^m \cdot X_j \right]}{\sum_{j=1}^{N} \left(u_{ij} \right)^m} \quad (i = 1, 2 \ldots C) \tag{4.4}$$

m (1, ∞) is a weighing component on each fuzzy membership. This weighing component controls the degree of fuzziness. The fuzziness of clustering depends on

value of *m* and it increases with increase in m. When *m*=1, clustering becomes hard. d^2 (x$_j$, v_i) is a function which measures the similarity between x$_j$ and v_i.

$$d^2 \cdot \left(X_j, V_i \right) = \left(\left| X_j - V_i \right| \right)^2 \tag{4.5}$$

$\left\| \bullet \right\|$ can be defined as either a straightforward Euclidean distance or its generalization such as the Mahalanbois distance (Taguchi, Chowdury and Wu, 2002).

The feature vector *X* in the FCM algorithm represents grey-levels of pixels because we are interested in the grey-level images. So, the feature vector only has one dimension where *p* is equal to one. The membership *U* and the cluster centre *V* are reduced to $N \times C$.

The FCM algorithm iteratively optimises function $J_m(U, V)$ with the continuous update of $U^{(1)}$ and $V^{(1)}$, where *l* stands for the number of iterations. The generalised steps of this algorithm can be given as below:

(1) Determine the number of clusters *C*, $2 \leq C \leq N$ and *m*.

(2) Randomly initialise the fuzzy membership $u_{ij}^{(0)}$ of x_j belonging to the *i*-th cluster.

(3) At the *l*-th iteration (*l* = 0, 1, 2…), calculate the cluster feature centre $v_i^{(l)}$ for *i* =1, 2,…. *C*.

(4) Calculate d^2(x$_j$, $v_i^{(l)}$).

(5) Update $u_{ij}^{(l)}$ with d^2(x$_j$, $v_i^{(l)}$).

(6) Compare $u_{ij}^{(l)}$ and $u_{ij}^{(l-1)}$,if $\| u_{ij}^{(l)} - u_{ij}^{(l-1)} \| < \varepsilon$, then stop, otherwise, *l*=*l*+1, go to step 3 and repeat.

At the end of all computations, each vector has a membership to each cluster and it is allocated to the cluster for which it shows the highest membership. In image segmentation, the cluster number *C* corresponds to the number of sub- regions into which the image is segmented. On segmentation pixel will most likely belong (separated) to the sub- region (cluster) to which it shows the highest membership.

The drawbacks of the FCM algorithm in image segmentation are easy to notice. Firstly, from eq. (4.2) it can be interpreted that the objective function of FCM does not take into consideration any spatial dependence among *X*, but deals with

images as totally separate points. Secondly, the membership function *U* (eq. (4.3)) is primarily derived from d^2 (x_j, v_i), this function calculates the similarity between the pixel intensity and cluster centre which shows the sensitivity of membership function to the noise. Problem occurs when an MR image to be segmented is noisy or is affected by artifacts, and then pixel intensities may be changed because of noise or artifacts. This may lead to incorrect membership and improper segmentation.

4.5 THEORETICAL COMPARISON BETWEEN FUZZY C-MEANS CLUSTERING ALGORITHM AND ITS EXTENSION

Segmentation comparison is an inter-technique process. The purpose of comparison for different algorithms is to rank their performance and to provide guidelines in choosing suitable algorithms according to applications as well as to promote new developments by effectively taking the strong points of several algorithms (Zhang, 1977). Comparison between FCM and its immediate extensions is discussed by Shen *et al* (2005). This comparison is of particular relevance here since it discusses a number of fuzzy-based segmentation algorithms. An inter-comparison of fuzzy-based segmentation algorithms is carried out later in this thesis. This section deals with similar comparisons in detail (Shen *et al.,* 2005).

Basically this section describes various attempts made by researchers to overcome the problems of the FCM algorithm, their approaches and to what extent these new improvements in FCM were successful in minimising the drawbacks of FCM.

Smoothing of the image before FCM segmentation may greatly improve the results. But use of standard smoothing filters may lead to a loss of important image details. Over the years researchers have proposed many extension of the FCM algorithm. Tolias and Panas (1998a) proposed post-processing of the membership function to smooth the effect of noise. Acton and Mukherjee (2000) and Tolias and Panas (1998b) incorporated multi-scale information to enforce spatial constraints.

Modification of the objective function can be said as most the most popular approach for improving the robustness of FCM. Dave (1991) introduced the idea of a noise cluster to handle noisy clustering data. The algorithm they proposed was named as nosing clustering algorithm (NC); in which the noise was clustered separately and excluded from the other clusters. NC algorithm is not appropriate for image

segmentation because noisy pixels should not be separated from the other pixels, rather they should be segmented into most appropriate clusters while reducing the effect of noise. Each pixel can belong to only single cluster. Use of NC algorithm for segmentation produces incomplete image because of elimination of noisy pixels from it.

A somewhat similar technique was put forward by Krishnapuram and keller (1993) known as possibilistic *c*-means algorithm (PCM). PCM interprets the clustering as a possibilistic partition. It works on a new objective function, in which a new term is introduced, which forces the membership as high as possible without a maximum limit constraint of one. Though the PCM algorithm may improve the working of clustering in a noisy environment, it does not have capability of dealing more widely with image segmentation. Because objective function is less strict in PCM, there is large possibility that the pixels will get stuck in one cluster. This indicates that for successful clustering of raw data, PCM needs specific requirements. This is major weakness of PCM algorithm.

Pham (2001) proposed the Robust Fuzzy C-Means (RFCM) algorithm. In RFCM, a new objective function was introduced incorporating spatial context into FCM. It "includes a penalty term that is reminiscent of MRF priors but consistent with the desired behaviour of the membership function…." (Pham 2001). As compared to the NC and PCM algorithms RFCM uses the neighbouring pixels for smoothing the effect of noise. But modification in objective function for reducing noise effect results in complex variation of the membership function. Ultimate results of all this are difficulty in computations and discontinuity from the original FCM technique.

As from the short review above, many improvements in FCM are being proposed via introduction of new algorithms but almost all had their own flaws. In the next section one more extension to the FCM is discussed.

4.6 IMPROVED FUZZY C-MEANS CLUSTERING (IFCM) ALGORITHM

The improved Fuzzy C-means (IFCM) clustering algorithm was introduced by Shen *et al* to overcome the drawbacks of FCM and its extension methods discussed in previous section (Shen *et al*., 2005). IFCM takes into consideration the attraction

between neighbouring pixels to reduce the effect of noise and artifacts in image segmentation.

The basis of IFCM is the following theory (Shen, 2004): It can be said that a single pixel is too small to represent a part in an image. If a pixel possesses a completely different intensity from its surrounding pixels, it will be reasonable to consider that this pixel is affected by noise. Real intensity of that pixel should be somewhat identical to its neighbour pixels. Therefore, an attraction can be supposed to exist between the nearby pixels. During clustering each pixel tries to attract its neighbouring pixels towards its own cluster. This attraction is named as neighbourhood attraction in the IFCM technique.

Further, neighbourhood attraction depends on two factors, firstly the pixel feature, and secondly the structure of neighbourhood. Pixel feature corresponds to the pixel intensity in grey-level images. Suppose a pixel has a very similar intensity to one of its neighbours, the attraction between them will be stronger than the attraction between the pixel and its neighbour with different intensity. Second factor, pixel structure, is the other important factor in determining the neighbourhood attraction. The closer neighbour pixel will have a stronger neighbour attraction as compared to farther neighbour. Neighbourhood components may also influence the attraction.

In summary, in the IFCM technique, the first component of the neighbourhood attraction, which depends on the pixel intensities, is called feature attraction, while the second component, which is based on the position of neighbours, is called distance attraction.

It is clear from the above description that, the membership value of FCM decides the segmentation results, in which the membership value is computed by the similarity measurement d^2 (x_j, v_i). It can be said that this measurement is the decisive factor in segmentation. In FCM, intensity difference between the pixel and the cluster centre is computed by d^2 (x_j, v_i) without considering the noise effects. But in contrary to that, IFCM considers the neighbourhood attraction in d^2 (x_j, v_i) directly. The extension to the equation is as follows:

$$d^2 \ (x_j, v_i) = \| \ x_j - v_i \| \ (1 - \lambda H_{ij} - \xi F_{ij}) \tag{4.6}$$

where H_{ij} represents the feature attraction and F_{ij} represents the distance attraction.

$$H_{ij} = \frac{\displaystyle\sum_{k=1}^{S} u_{ik} \cdot g_{jk}}{\displaystyle\sum_{k=1}^{S} g_{jk}} \qquad (4.7)$$

In equation g_{jk} is the intensity difference between the study pixel j and its neighbour pixel k.

$$g_{jk} = \left| X_j - X_k \right| \qquad (4.8)$$

u_{ik} is the membership of the neighbour pixel k to the i-th cluster. S is the number of neighbour pixels.

$$F_{ij} = \frac{\displaystyle\sum_{k=1}^{S} (u_{ik})^2 \cdot (q_{jk})^2}{\displaystyle\sum_{k=1}^{S} (q_{jk})^2} \qquad (4.9)$$

where q_{jk} is the relative location between the pixel j and its neighbour pixel k. In a two dimensional image, j and k only refer to the name of the pixel, not the actual location.

IFCM works similarly to that of traditional FCM, only with the modification of $d^2(x_j, v_i)$. The initialisation of the membership is inherited from FCM, as a reason FCM is executed firstly before implementing IFCM. The final memberships obtained from FCM are used as initial membership for IFCM, which also reduces the computation time greatly. IFCM works with following steps:

(1) Determine the number of clusters C $(2 \leq C \leq N)$ and m

(2) Execute FCM completely

(3) Utilize the final membership of FCM as the initial membership

(4) At the l-th iteration (l=0,1,2…), calculate the cluster centre $v_i^{(l)}$ (i = 1,2….C) using the membership $u_{ij}^{(l)}$

(5) Calculate the improved similarity measurement $d^2(x_j, v_i^{(l)})$

(6) Update $u_{ij}^{(l)}$ with $d^2(x_j, v_i^{(l)})$

(7) Compare $u_{ij}^{(l)}$ and $u_{ij}^{(l-1)}$, if $u_{ij}^{(l)} - u_{ij}^{(l-1)} < \varepsilon$, then stop, otherwise, l =l+1, go to step 4 and repeat.

CHAPTER 5

DATA COLLECTION

Firstly, data in this thesis specifically refers to MRI brain images only, since MRI brain images were only and main object of study in this thesis.

5.1 DATA SOURCE

Type of data used for evaluating and comparing segmentation algorithms is very important. Since type of data used determines or leads to the corresponding segmentation results and the conclusions based on them.

Real image presented in this thesis was obtained from a website (Hornak, 2007). In the case of real MRI images, ground truth (reference data) is usually not available, which makes it very difficult to evaluate segmentation performance quantitatively. But evaluation and comparison of segmentation performance is possible visually (which is called qualitative comparison). Therefore, real MRI images were used for performing qualitative comparison of segmentation algorithms. Quantitative comparison of algorithms was possible with the help of Brainweb (http://www.bic.mni.mcgill.ca/brainweb/). Brainweb provides a simulated brain database (SBD); the SBD contains a set of realistic MRI data volumes produced by an MRI simulator. These data enable us to evaluate the performance of various image analysis methods in a setting where the truth is known {the precise regions of white matter, gray matter, CSF} (Brainweb, 2006; Kwan, 1999; Collins; Corcosco, 1997).

Therefore, for performing quantitative comparison between different segmentation algorithms, simulated brain images from the above source (Brainweb) were used in thesis, where ground truth is known.

5.2 DATA TYPE

All images used for this thesis are gray-level and two-dimensional images only. Out of many real images used for testing, results of only one real image are presented in this thesis (because of space constraint), whilst all other images are simulated.

5.3 DATA PARAMETERS

As all images used for this thesis were MRI images, data parameters refer to specifically MRI parameters. Real image used in this thesis was obtained from an actual examination recorded on a 1.5 Tesla, GE (Milwaukee, WI) Sigma magnetic resonance imager 44. As mentioned previously simulated images used in this thesis were obtained from SBD; SBD enables us to choose various MRI parameters, based on which simulated image was generated.

Brainweb provides following choice of MRI parameters. Parameters of simulated MRI images, which were used for this thesis, are mentioned along with the images in the result section.

Pulse sequences (PS): T_1 weighted, T_2 weighted, PD

Slice thickness (ST): 1mm, 3mm, 5mm, 7mm, and 9mm.

Noise (N): 0%, 1%, 3%, 5%, 7%, and 9%.

MRI artifact used: RF Inhomogeneity (RF Inhomo): 0%, 20%, and 40%.

Definitions and technical specifications of all MRI parameters used for generation of simulated brain images from SBD can be obtained from Brainweb, frequently asked questions section

(http://www.bic.mni.mcgill.ca/brainweb/faq.html).

CHAPTER 6
RESULTS AND COMPARISON

The aim of this thesis was to compare different segmentation algorithms. Qualitative comparison was performed on real MRI images and quantitative comparison was performed on simulated MRI images. For comparisons, four algorithms were written in MATLAB®, namely edge-based segmentation, K-means clustering, FCM and IFCM. All these algorithms were tested with simulated and real MRI images. This section firstly presents results of segmentation of all four algorithms for simulated images, followed by the results for the real image. After segmentation results of simulated and real images, qualitative and quantitative comparisons are performed and presented in the next section.

6.1 RESULTS FOR SIMULATED IMAGES

6.1.1 Edge-Based Segmentation

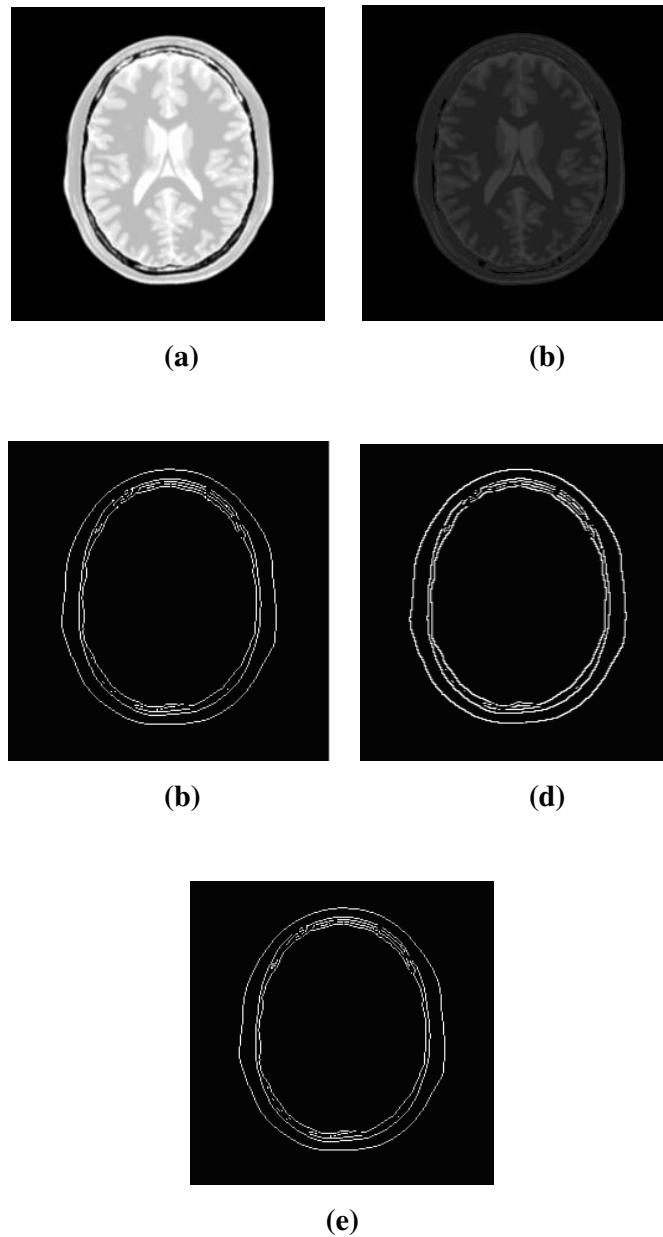- Parameters for input image **Figure 6.1(a):** PD, ST: 1mm, N: 0%, RF Inhomo: 0%.

(a)   **(b)**

(b)   **(d)**

(e)

Figure 6. 1 (a) Original image; **(b)** Result of normalisation applied on original image; **(c)** Result of gradient based Prewitt filter application on normalised image;

(d) Result of gradient based Roberts filter application on normalised image; **(e)** Result of gradient based Sobel filter application on normalised image. **Comment on segmentation result above**: All Prewitt, Roberts and Sobel filters shown poor results in segmenting PD weighted image, especially incapability in segmenting internal features (edges) of normalised PD weighted image. In other words, it can be stated as gradient edge based segmentation technique performed poorly on proton density images because of the subdued image intensities in PD weighted image.

- Parameters for input image **Figure 6. 2(a):** T_1, ST: 1mm, N: 0%, RF Inhomo: 0%.
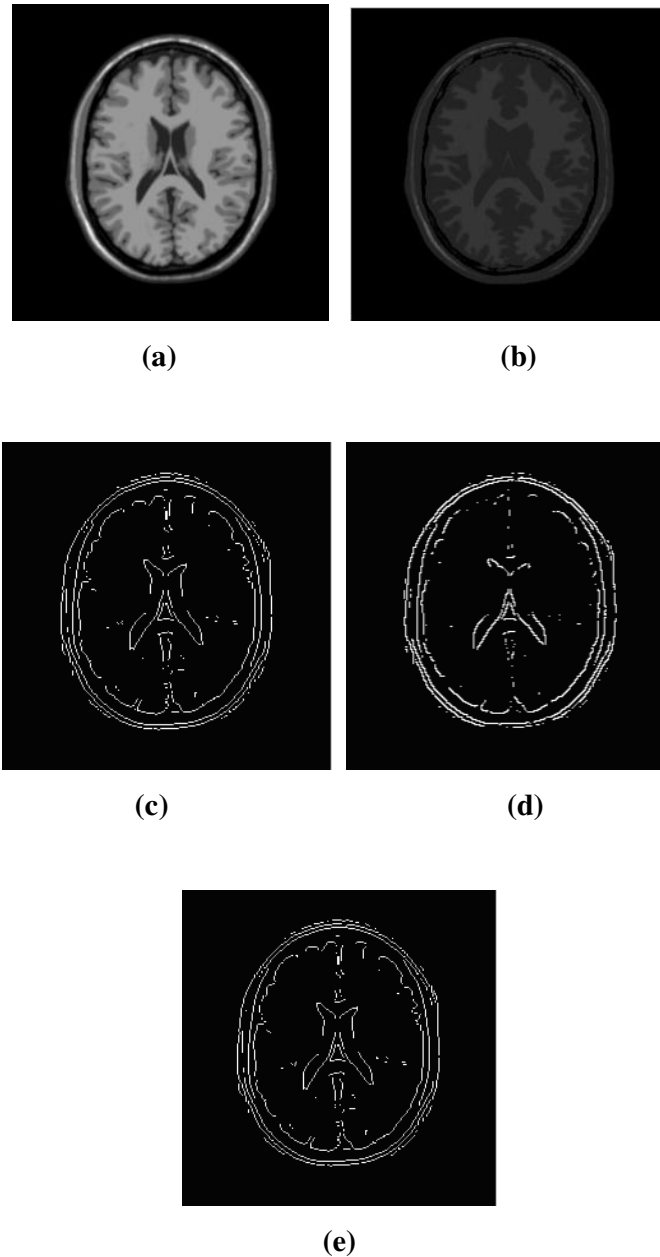

(a)   **(b)**

(c)   **(d)**

(e)

Figure 6. 2 (a) Original image; **(b)** Result of normalisation applied on original image; **(c)** Result of gradient based Prewitt filter; **(d)** Result of gradient based Roberts filter; **(e)** Result of gradient based Sobel filter.

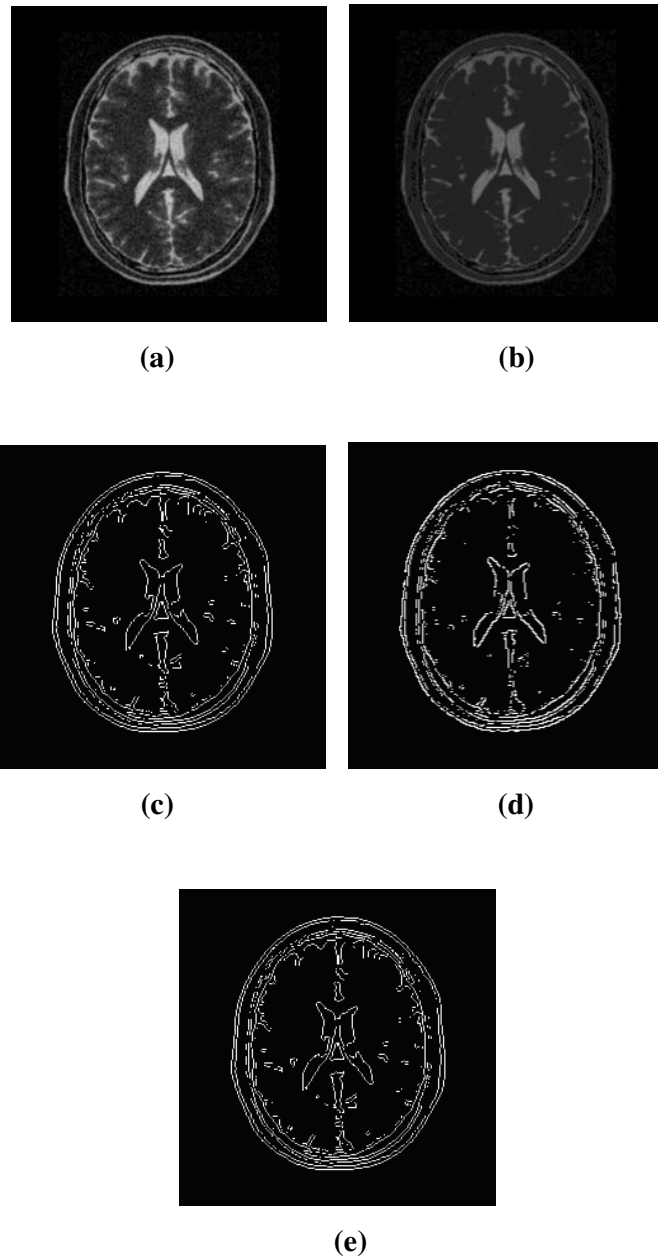- Parameters for input image **Figure 6. 3(a):** T_2, ST: 1mm, N: 9%, RF Inhomo: 40%.

(a)   **(b)**

(c)   **(d)**

(e)

Figure 6. 3 (a) Original image; **(b)** Result of normalisation applied on original image; **(c)** Result of gradient based Prewitt filter application; **(d)** Result of gradient based Roberts filter application; **(e)** Result of gradient based Sobel filter application.

6.1.2 K-Means Clustering

- Parameters input image **Figure 6. 4(a):** PD, ST: 1mm, N: 0%, RF Inhomo: 0%.
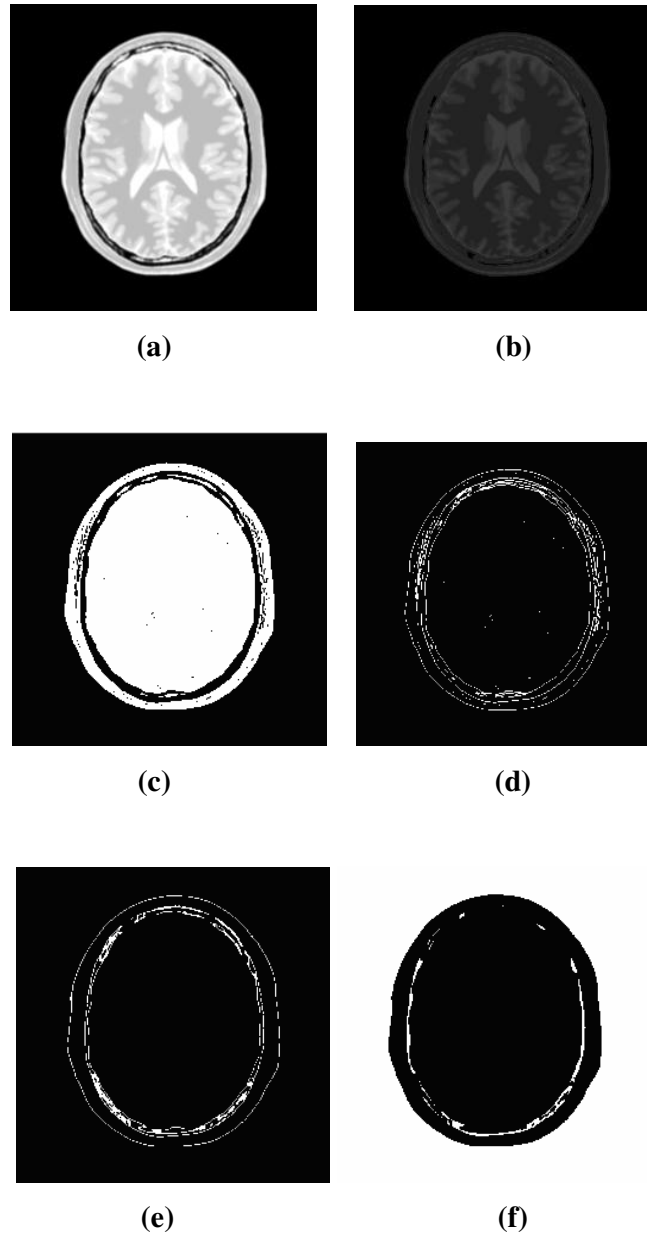

(a)	**(b)**
(c)	**(d)**
(e)	**(f)**

Figure 6. 4 (a) Original image; **(b)** Result of normalisation applied on original image; **(c)** Segmented cluster of White matter; **(d)** Segmented cluster of Gray matter; **(e)** Segmented cluster of CSF, **(f)** Segmented cluster of Skull.

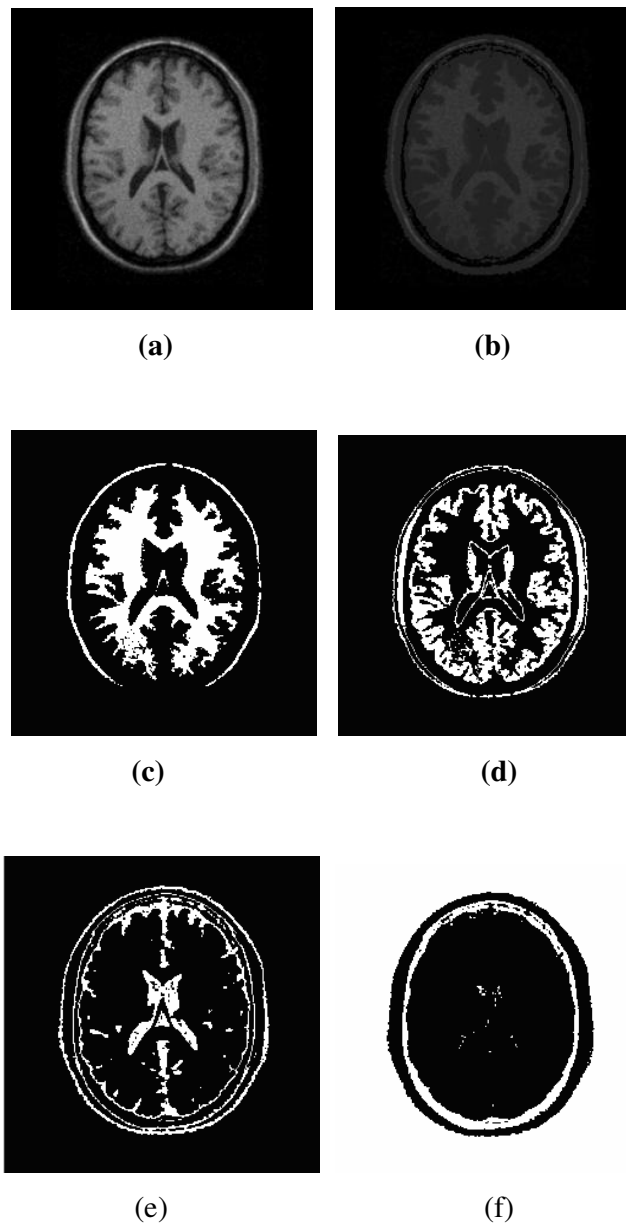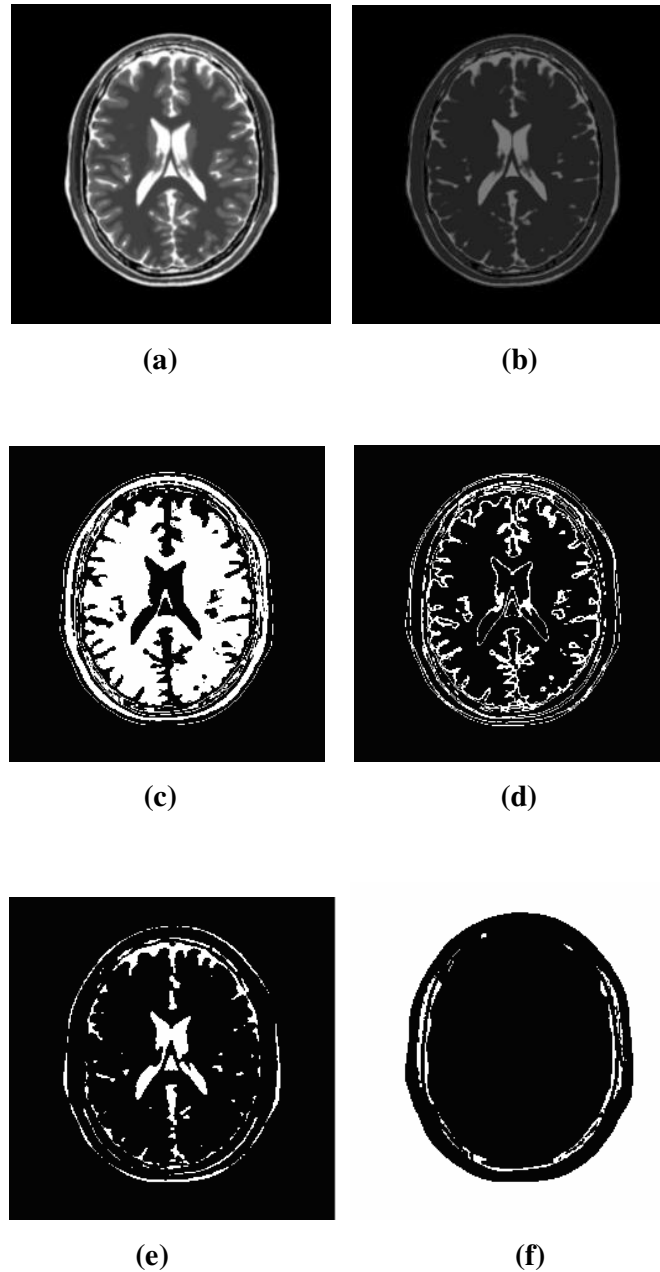Parameters for input image **Figure 6. 5(a):** T_1, ST: 1mm, N: 9%, RF Inhomo: 40%.

(a)   **(b)**

(c)   **(d)**

(e)   (f)

Figure 6. 5 (a) Original image; **(b)** Result of normalisation applied on original image; **(c)** Segmented cluster of White matter; **(d)** Segmented cluster of Gray matter; **(e)** Segmented cluster of CSF, **(f)** Segmented cluster of Skull

- Parameters for input image **Figure 6. 6(a):** T_2, ST: 1mm, N: 0%, RF Inhomo: 0%.

(a)   **(b)**

(c)   **(d)**

(e)   **(f)**

Figure 6. 6 (a) Original image; **(b)** Result of normalisation applied on original image; **(c)** Segmented cluster of White matter; **(d)** Segmented cluster of Gray matter; **(e)** Segmented cluster of CSF, **(f)** Segmented cluster of Skull

6.1.3 FCM

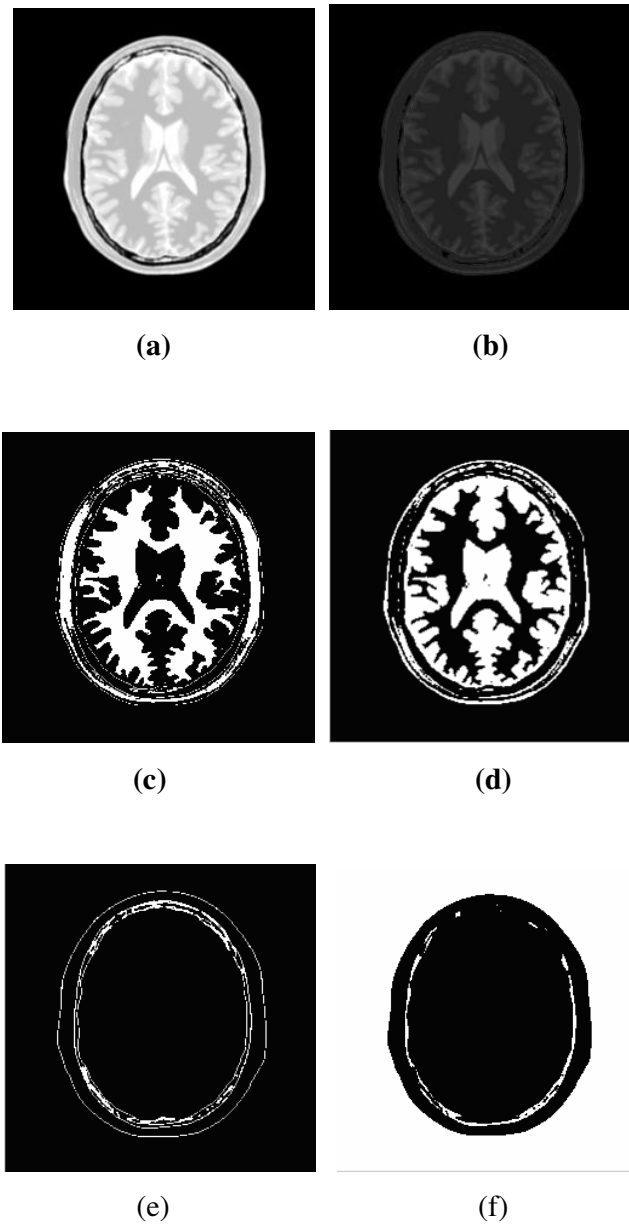- Parameters for input image **Figure 6. 7(a):** PD, ST: 1mm, N: 0%, RF Inhomo: 0%

(a)   (b)

(c)   **(d)**

(e)   (f)

Figure 6. 7 (a) Original image; **(b)** Result of normalisation applied on original image; **(c)** Segmented cluster of White matter; **(d)** Segmented cluster of Gray matter; **(e)** Segmented cluster of CSF, **(f)** Segmented cluster of Skull

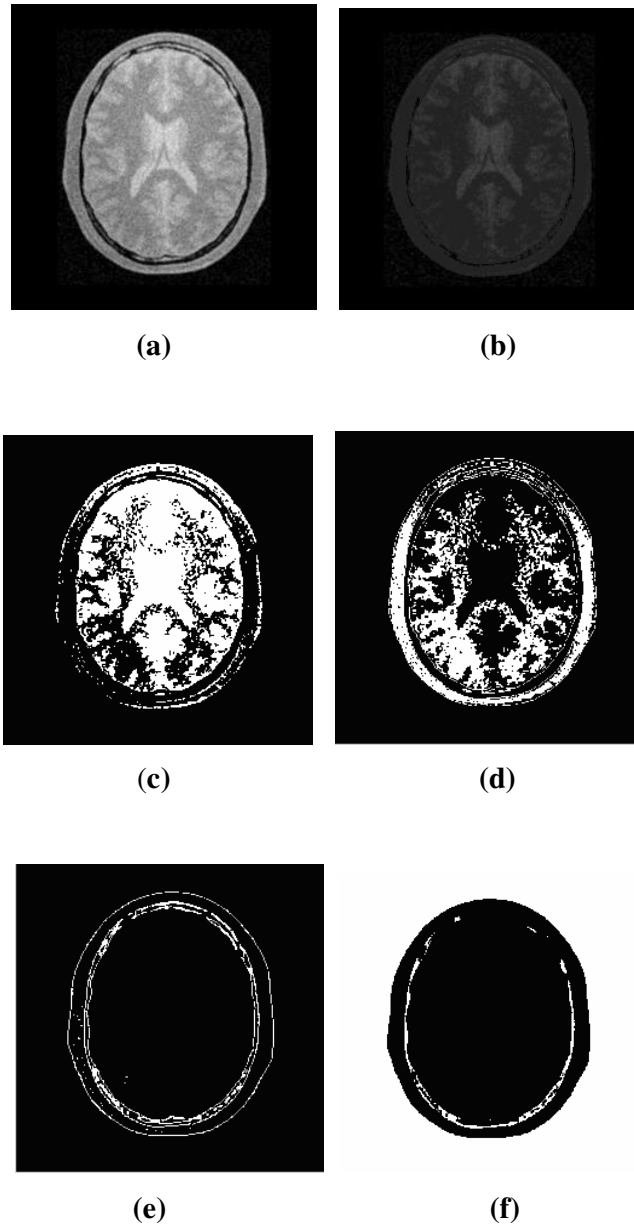- Parameters for input image **Figure 6. 8(a):** PD, ST: 1mm, N: 9%, RF Inhomo: 40%.

(a)   **(b)**

(c)   **(d)**

(e)   **(f)**

Figure 6. 8 (a) Original image; **(b)** Result of normalisation applied on original image; **(c)** Segmented cluster of White matter; **(d)** Segmented cluster of Gray matter; **(e)** Segmented cluster of CSF; **(f)** Segmented cluster of Skull

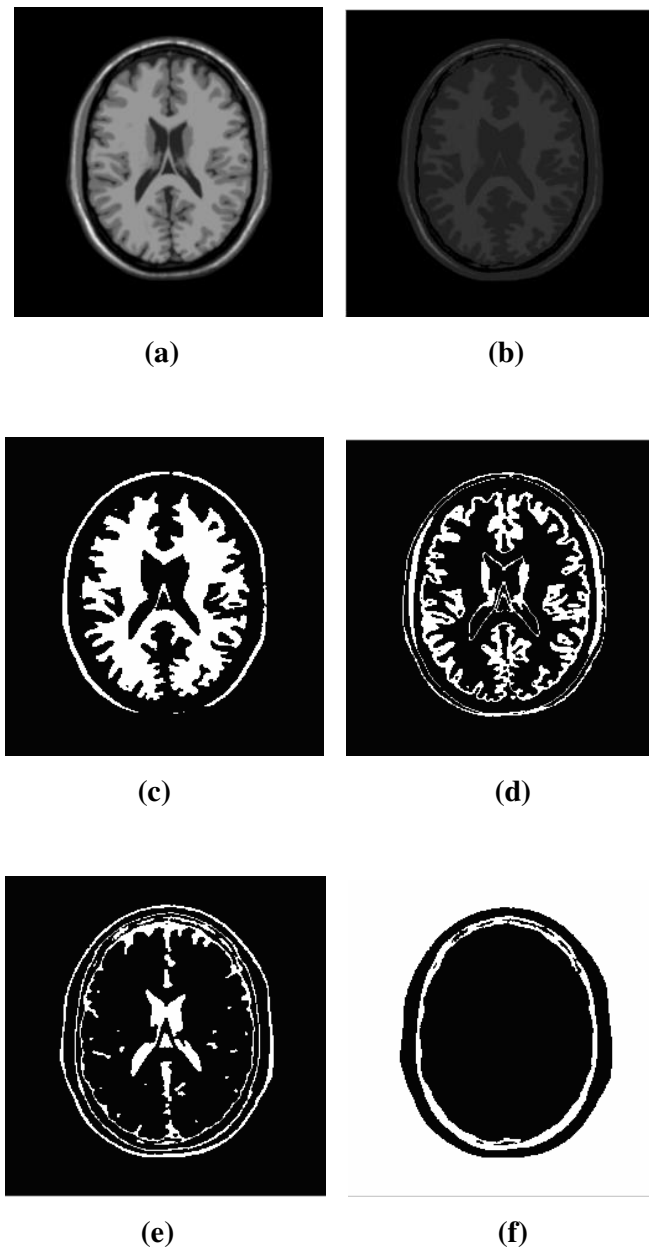- Parameters for input image **Figure 6. 9(a):** T_1, ST: 1mm, N: 0%, RF Inhomo: 0%

(a)   **(b)**

(c)   **(d)**

(e)   **(f)**

Figure 6. 9 (a) Original image; **(b)** Result of normalisation applied on original image; **(c)** Segmented cluster of White matter; **(d)** Segmented cluster of Gray matter; **(e)** Segmented cluster of CSF, **(f)** Segmented cluster of Skull

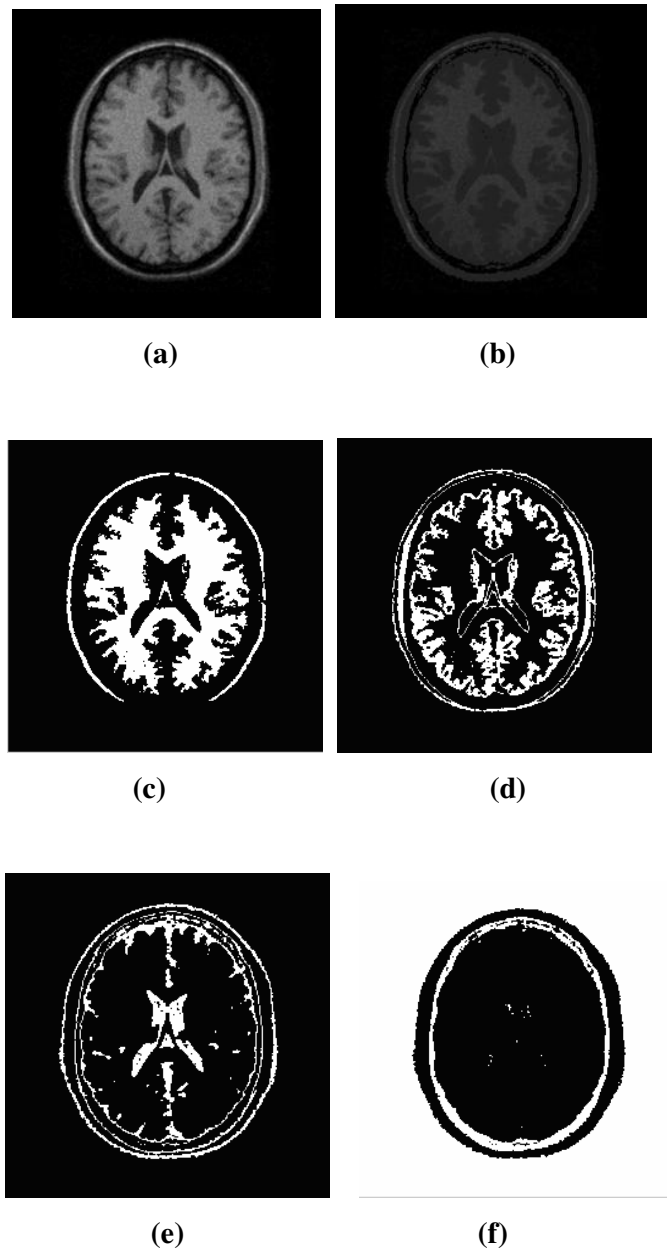- Parameters for input image **Figure 6. 10(a)** T_1, ST: 1mm, N: 9%, RF Inhomo: 40%.

(a)   **(b)**

(c)   **(d)**

(e)   **(f)**

Figure 6. 10 (a) Original image; **(b)** Result of normalisation applied on original image; **(c)** Segmented cluster of White matter; **(d)** Segmented cluster of Gray matter; **(e)** Segmented cluster of CSF, **(f)** Segmented cluster of Skull

- Parameters for input image **Figure 6. 11(a).** T_2, ST: 1mm, N: 9%, RF Inhomo: 40%.
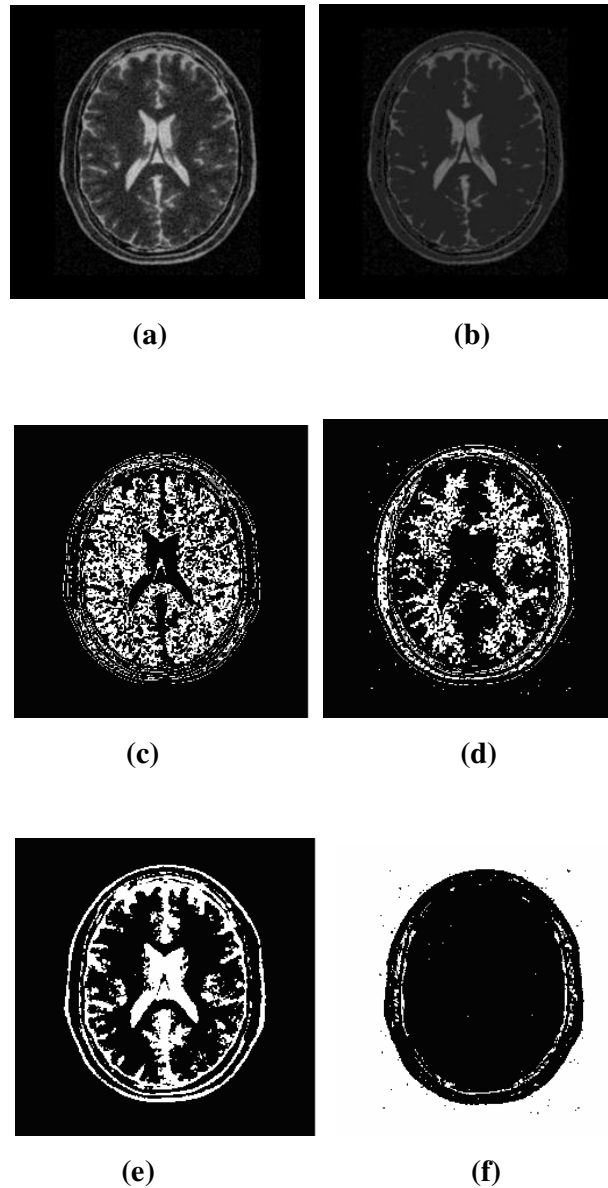

(a)   (b)

(c)   (d)

(e)   (f)

Figure 6. 11 (a) Original image; **(b)** Result of normalisation applied on original image; **(c)** Segmented cluster of White matter; **(d)** Segmented cluster of Gray matter; **(e)** Segmented cluster of CSF, **(f)** Segmented cluster of Skull

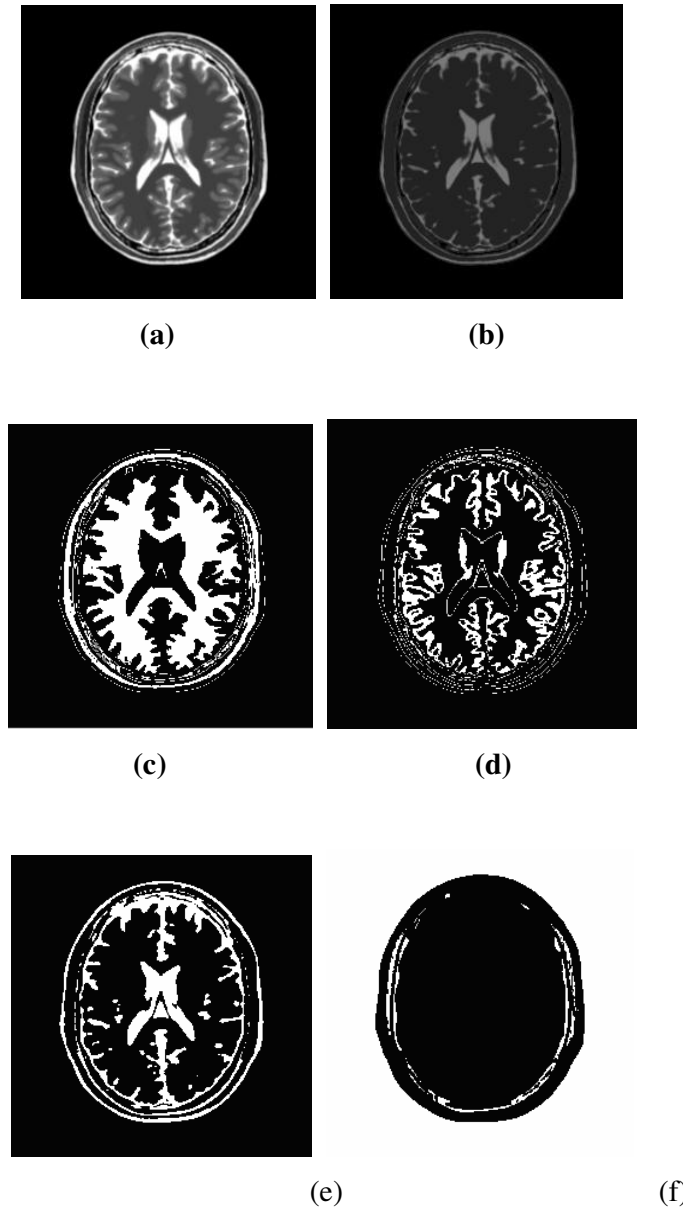- Parameters for input image **Figure 6. 12(a):** T_2, ST: 1mm, N: 0%, RF Inhomo: 0%.

(a)   **(b)**

(c)   **(d)**

(e)   (f)

Figure 6. 12 (a) Original image; **(b)** Result of normalisation applied on original image; **(c)** Segmented cluster of White matter; **(d)** Segmented cluster of Gray matter; **(e)** Segmented cluster of CSF, **(f)** Segmented cluster of Skull

6.1.4. IFCM

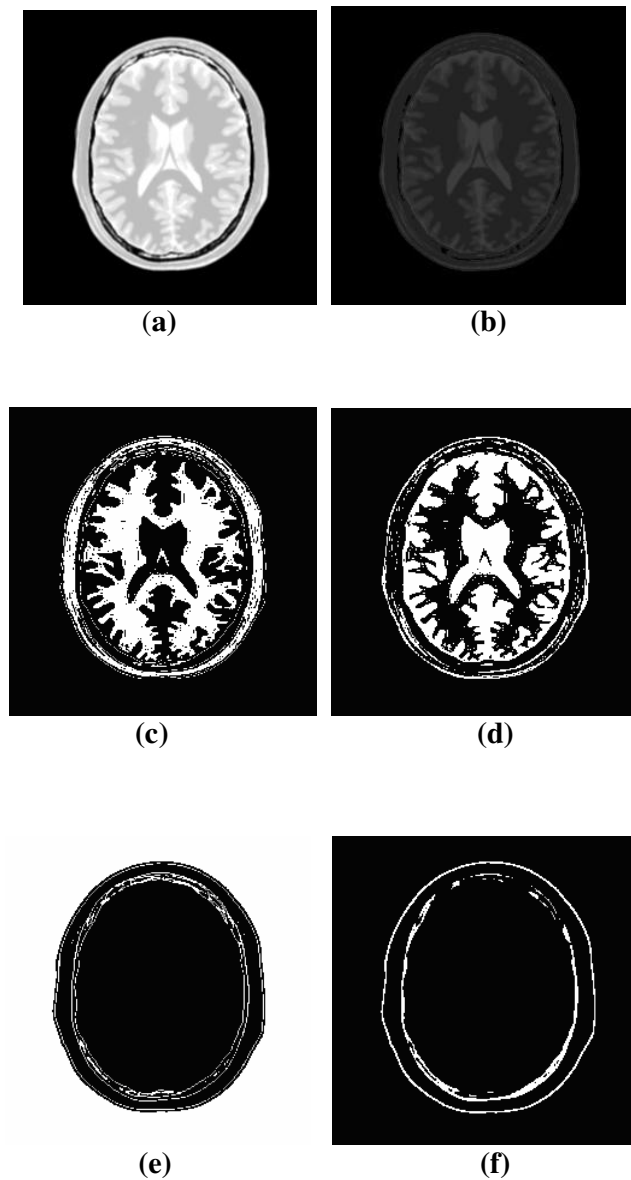- Parameters for input image **Figure 6. 13(a):** PD, ST: 1mm, N: 0%, RF Inhomo: 0%.

(**a**)   (**b**)

(**c**)   (**d**)

(**e**)   (**f**)

Figure 6. 13 (**a**) Original image; (**b**) Result of normalisation applied on original image; (**c**) Segmented cluster of White matter; (**d**) Segmented cluster of Gray matter; (**e**) Segmented cluster of CSF, (**f**) Segmented cluster of Skull

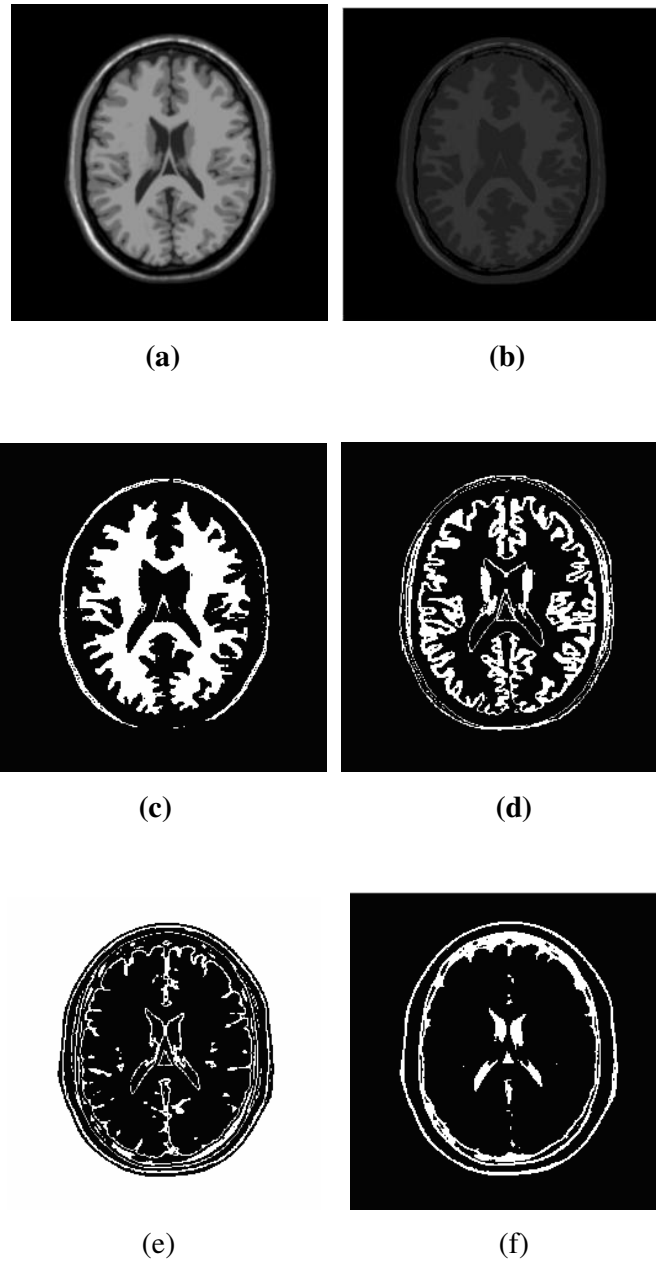- Parameters for input image **Figure 6. 14(a):** T_1, ST: 1mm, N: 0%, RF Inhomo: 0%.

(a)   (b)

(c)   (d)

(e)   (f)

Figure 6. 14 (a) Original image; **(b)** Result of normalisation applied on original image; **(c)** Segmented cluster of White matter; **(d)** Segmented cluster of Gray matter; **(e)** Segmented cluster of CSF, **(f)** Segmented cluster of Skull

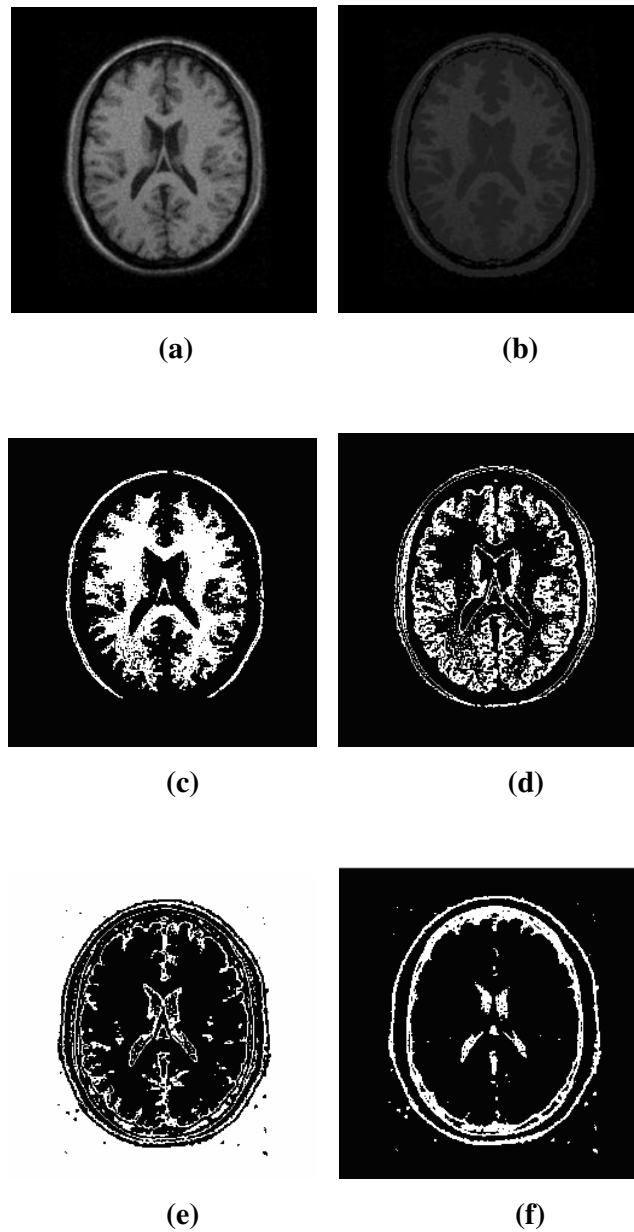Parameters for input image Figure 6. 15(a): T_1, ST: 1mm, N: 9%, RF Inhomo: 40%.

(a)   **(b)**

(c)   **(d)**

(e)   **(f)**

Figure 6. 15 (a) Original image; **(b)** Result of normalisation applied on original image; **(c)** Segmented cluster of White matter; **(d)** Segmented cluster of Gray matter; **(e)** Segmented cluster of CSF; **(f)** Segmented cluster of Skull

6.2 RESULTS FOR REAL IMAGES

6.2.1 Edge-Based Segmentation

(a)

(b)   **(c)**
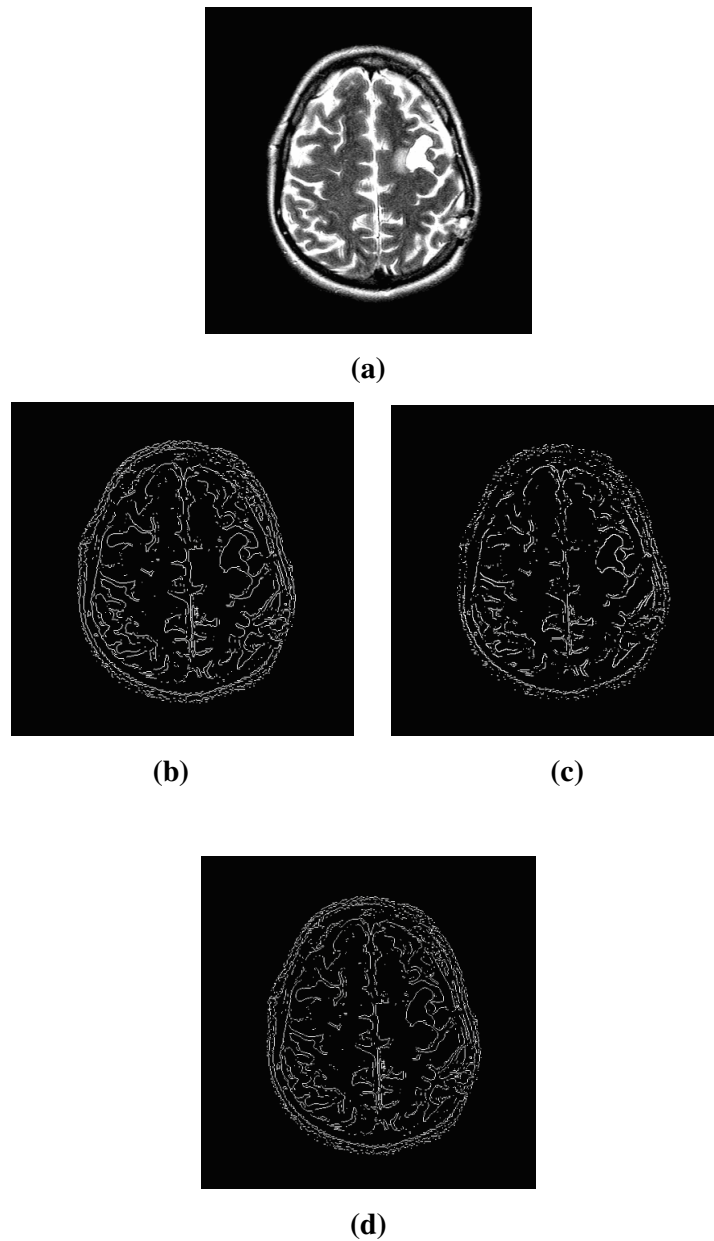

(d)

Figure 6. 16 (a) Original image; (**b**) Result of gradient based Prewitt filter application on original image; (**c**) Result of gradient based Roberts filter application on original image; (**d**) Result of gradient based Sobel filter application on original image
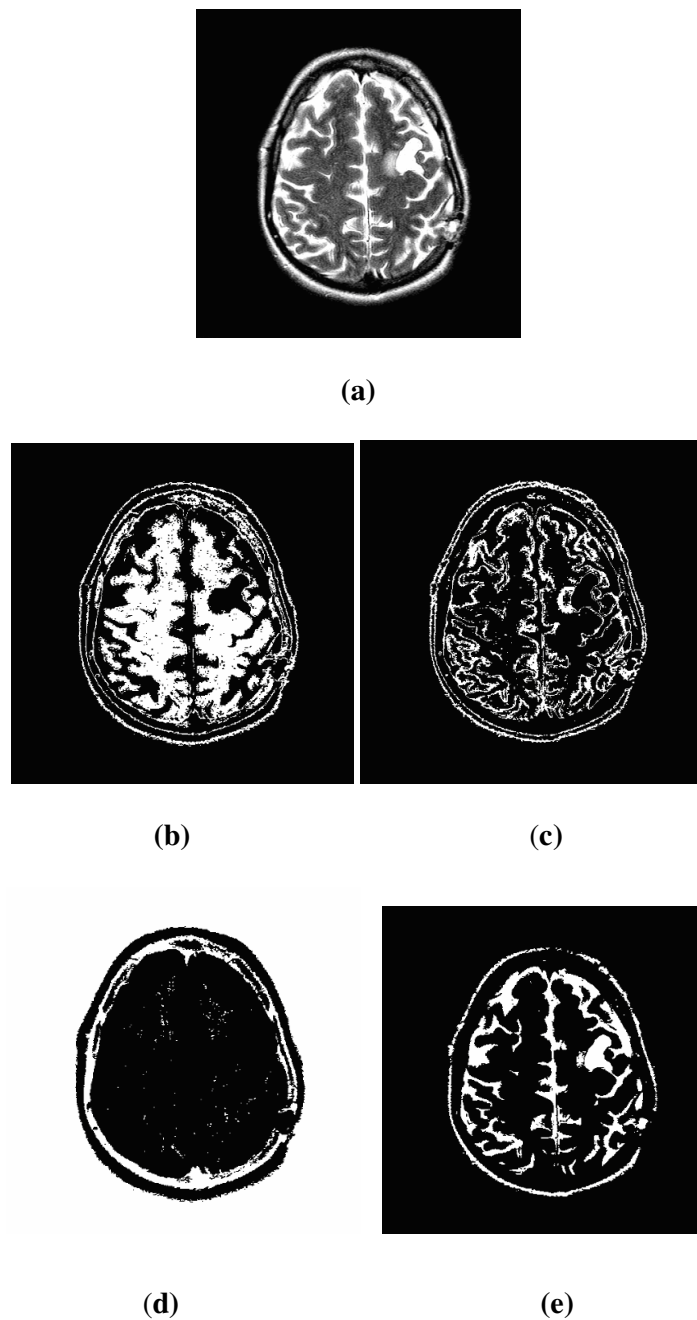
6.2.2 K-means Clustering Segmentation

(a)

(b)   (c)

(d)   (e)

Figure 6. 17 (**a**) Original image; (**b**) Segmented cluster of White matter after application of K-means; (**c**) Segmented cluster of Gray matter after application of K-means; (**d**) Segmented cluster of CSF after application of K-means; (**e**) Segmented cluster of Skull after application of K-means
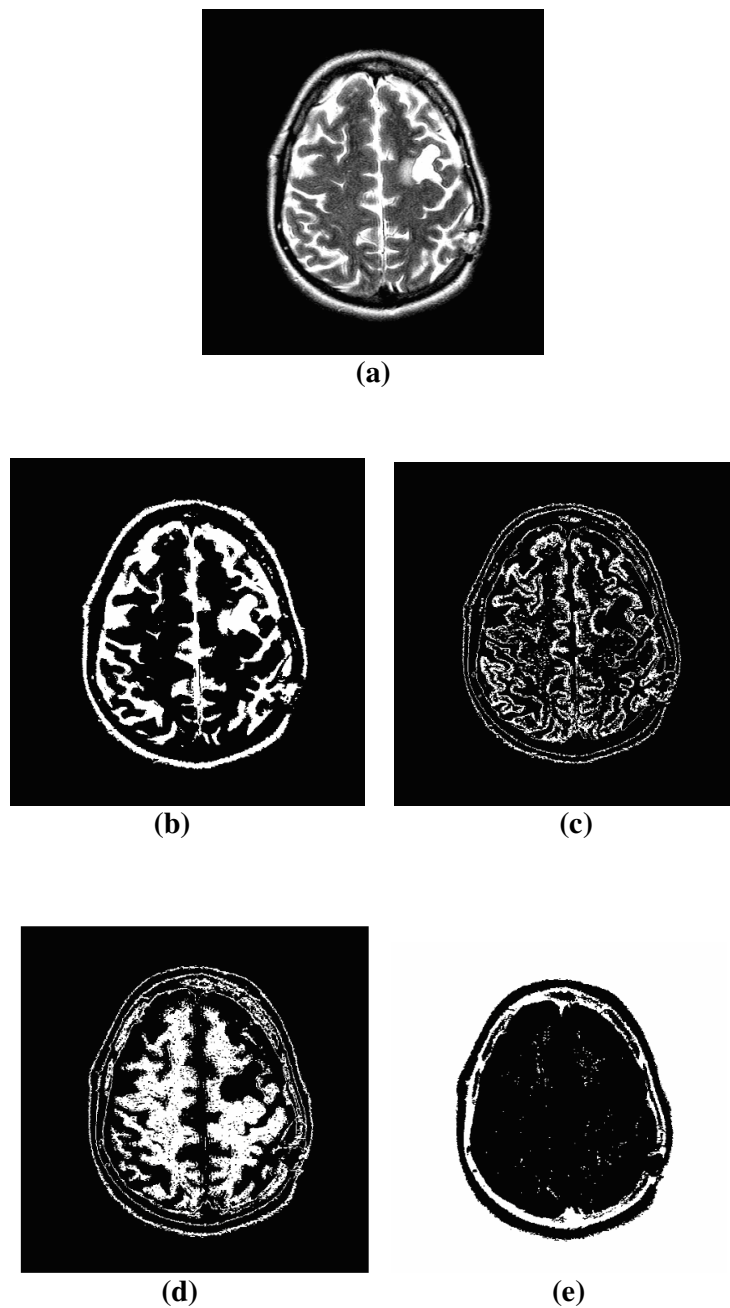
6.2.3 FCM Clustering Segmentation

(a)

(b)

(c)

(d)

(e)

Figure 6. 18 (a) Original image; (**b**) Segmented cluster of White matter after application of FCM; (**c**) Segmented cluster of Gray matter after application of FCM; (**d**) Segmented cluster of CSF after application of FCM; (**e**) Segmented cluster of Skull after application of FCM
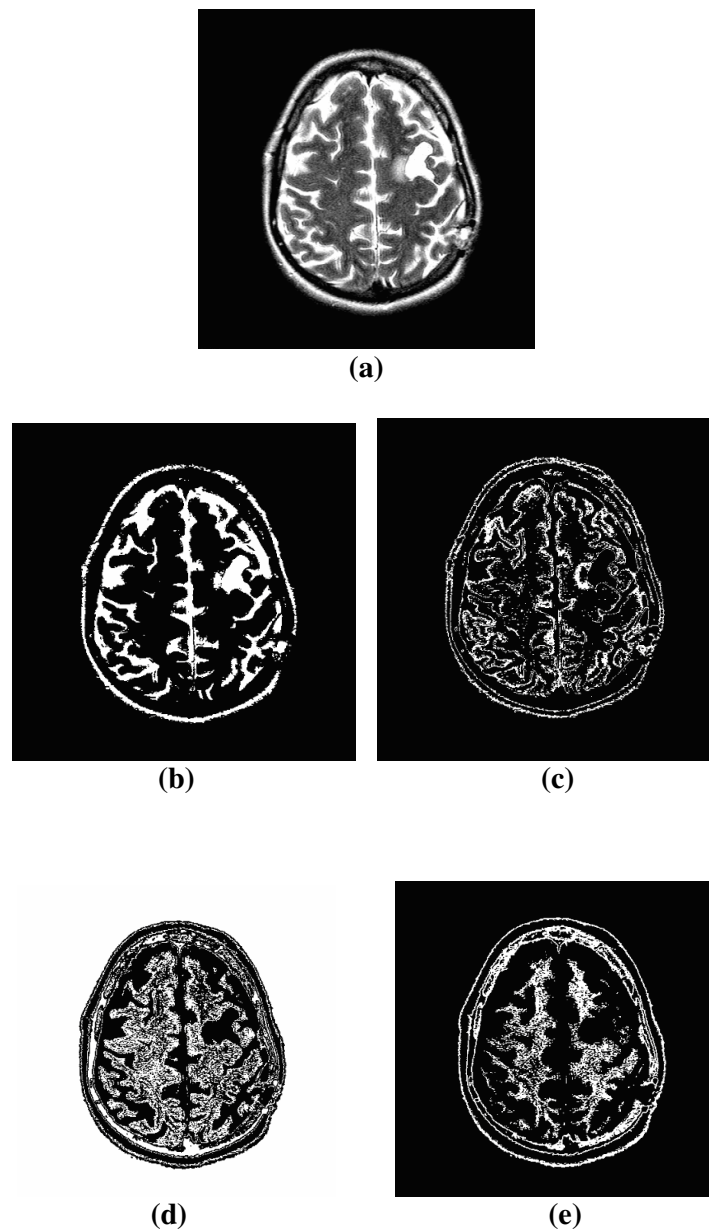
6.2.4 IFCM clustering segmentation

Figure 6. 19 **(a)** Original image; **(b)** Segmented cluster of White matter after application of IFCM; **(c)** Segmented cluster of Gray matter after application of IFCM; (**d**) Segmented cluster of CSF after application of IFCM; **(e)** Segmented cluster of Skull after application of IFCM

6. 3 COMPARISIONS

6.3.1 Qualitative comparison

Based on the results obtained from the segmentation of the real MRI images, qualitative comparison was done visually. Results of the comparison are presented in tabular form below. Edge- based segmentation, K-means clustering, Fuzzy C-means clustering and Improved fuzzy C-means clustering were used for inter-comparison.

Table 6.1: Qualitative comparison between algorithms

	Edge-based segmentation	**K-means clustering**	**Fuzzy C-Means clustering**	***Improved fuzzy C-means clustering**
Performance on segmentation of clusters	Poor	Good	Very good	Good
Sensitivity to noise	Low	Sensitive	Sensitive	Sensitive
(Algorithm) Computation time	Short	Long (average among all)	Long	Long
Simplicity in implementing algorithm.	Very simple	Difficult	Difficult	Difficult
Nature of algorithm	Not applicable	Unsupervised	Unsupervised	Unsupervised
Feasibility of using in practical (clinical environment)	Can not be used	Average performance, but not very robust in all cases	Can be used	Can be used. Can work more efficiently if implemented/ written accurately

*Above comments made about the performance of IFCM are not accurate because of limitations in implementing the complete code of IFCM algorithm in MATLAB. This issue and its reason are discussed clearly in the following 'conclusions and future work' section.

       As mentioned above qualitative comparison was done visually. It was done by comparing the segmentation results of the above mentioned four algorithms with each other, i.e. segmentation result obtained by segmenting real MRI image was compared with original image to see how precisely the segmentation algorithm has segmented the clusters i.e. gray matter, white matter, CSF and skull.

       Further, segmentation results (performances) of segmentation algorithms were compared among each other (among four algorithms) to rate them as poor, good and very good (among themselves). Here poor means, worst performance of all algorithms which also signifies algorithm's incapability in segmenting brain MRI images into gray matter, white matter, CSF and skull. Good means, algorithm is fairly capable of segmenting brain MRI images into clusters. Very good, means algorithm performed best segmentation among all (four algorithms) and precisely segmented the clusters of gray matter, white matter, CSF and skull.

       For judging the segmentation performance of algorithms; it is worthwhile to mention that much better qualitative (analysis) results could have been obtained from (3/4) clinical experts, who can analyse and evaluate image segmentation results.

6.3.2 Quantitative comparison

Quantitative comparison between four segmentation algorithms was performed with the help of simulated images. For carrying out quantitative comparison, the following criteria was used,

    Results of segmentation (obtained from simulated images) of each algorithm were compared with the original simulated images (Since simulated images were used it was possible to know precisely the original segmentation region which each pixel in the various regions belongs to).

    For precise quantitative comparison two parameters were used for counting the number of pixels from segmented images, which are given below.

_CS_ (correct segmentation): Number of pixels, which were segmented correctly in the particular cluster in comparison with corresponding cluster from original simulated image.

InCS (incorrect segmentation): Number of pixels, which were segmented incorrectly in the particular cluster in comparison with corresponding cluster from original simulated image.

Using the above mentioned technique quantitative comparison was performed by counting the number of correctly and incorrectly segmented pixels in segmented image and its corresponding original simulated image. This was done with MATLAB® software. The results obtained are displayed in the form of percentage of correct segmentation and incorrect segmentation.

Results obtained are displayed in tabular form below.

Table 6.2: Quantitative comparison between algorithms

Results on images without noise and artifact				
	Edge- based segmentation	**K- means segmentation**	**FCM segmentation**	***IFCM segmentation**
Correct - segmentation	26.6%	88.0%	91.1%	86.3%
Incorrect segmentation	Not applicable	9.4%	8.7%	12.7%
Results on images with noise and artifact				
Correct - segmentation	24.3%	86.2%	88.7%	84.9%
Incorrect segmentation	Not applicable	9.9%	9.4%	13.5%

*Above comments made about the performance of IFCM are not accurate because of limitations in implementing the complete code of IFCM algorithm in MATLAB. This issue and its reason are discussed clearly in the following 'conclusions and future work' section.

It will be worthwhile to mention here that looking at the comparison table above; apparently there is not big difference in percentages of correct and incorrect segmentation among above four algorithms. Though it is so, this small difference in

(percentage) figures makes substantial difference in actual segmentation when looked at visually. These (quantitative) results are supported by qualitative results. In other words results of qualitative and quantitative comparisons were complementary to each other.

CHAPTER 7
CONCLUSIONS AND FUTURE WORK

7.1 Conclusions

As mentioned in previous sections, the objective of this thesis was to perform inter-comparison of segmentation algorithms. This objective was achieved by carrying out qualitative comparison on real images and quantitative comparison on simulated images. In the previous section both qualitative and quantitative comparisons were presented.

Results of both qualitative and quantitative comparisons can be taken as fair representation of performance of algorithms in segmenting MRI brain images, with the exception of IFCM algorithm. Since authors (Shen *et al*., 2005) who proposed IFCM algorithm, have used neural network technique for determination of two important parameters involved in the IFCM algorithm, namely λ and ξ; and development of neural network for determining these two parameters for IFCM algorithm was out of scope of this thesis. Therefore, these parameters (λ, ξ) were chosen randomly. But random choice of these parameters is not correct solution; rather it degraded the segmentation results. As IFCM algorithm written and implemented for this thesis was incomplete IFCM algorithm (without precise values of parameters λ, ξ); therefore segmentation results of it cannot be taken as reliable results for precise comparison with other algorithms.

Both qualitative and quantitative comparisons confirmed superiority of fuzzy based algorithms over classical algorithms. Edge based segmentation shown the poorest performance of all, K-means performed better, IFCM also performed better (though it had above discussed issue), and FCM performed best among all.

Comparisons between above four algorithms facilitated very useful information, which resulted into following conclusions.

- Classical segmentation algorithm, like edge-based segmentation cannot be used as a primary or sole segmentation technique for segmenting (complex) images like brain MRI images. If it is to be used at all, then it should be used along with other segmentation techniques. Another drawback of edge based segmentation

technique is that, it does not segment image into different clusters (as it is not clustering algorithm), which makes it really hard to understand segmented image even though it is segmented precisely. Overall segmentation results of edge-based segmentation were very poor displaying total incapability of this technique in handling complex image data like brain MRI images.

- K-means clustering algorithm performed much better segmentation than edge based segmentation algorithm. One drawback of K-means algorithm was, it performed large amount of incorrect segmentation. Secondly, K-means cannot work in noisy conditions, which decreases its robustness in overall segmentation.

- IFCM clustering algorithm undoubtedly performed better than edge-based segmentation algorithm and almost similar to K-means clustering algorithm. But as discussed previously, results of IFCM segmentation (in this thesis) are not accurate, so commenting on the performance of IFCM algorithm will be totally wrong.

- FCM clustering algorithm displayed the best performance of all proving the superiority of fuzzy approach in segmenting complex and vague data such as brain MRI images. FCM algorithm shown good results in noisy conditions also, indicating its robustness as segmentation technique.

- One more very important factor is MR image pre-processing. As objective of this thesis was inter-comparison of segmentation algorithms therefore MR image pre-processing was out of scope of this thesis. But results of segmentation above have indicated that, MR image pre-processing is unavoidable process. In many cases in this thesis, background of the image was also segmented along with the image. Removal of background pixels, removal of non-brain region and image standardisation will certainly improve the results of segmentation.

- For better comparison among various algorithms, grouping technique may prove useful. Such as, classical algorithms can be grouped in one group, fuzzy based algorithms in other and statistical algorithms in another group. This type of grouping of algorithms based on their technique (classical, fuzzy or statistical) will display overall performance of that technique in segmenting images and further in that group algorithms can be ranked according to their performance.

- Unfortunately, there was no concrete and reliable information available on World Wide Web regarding which image segmentation techniques are being used in state of the art commercial (medical) MRI equipments. However, during the course of this thesis, whatever (recent) peer reviewed journals and research papers were studied, based on that knowledge it will be fair to suggest that for (brain) MRI image segmentation fuzzy based clustering is the most widely used and researched segmentation technique now a days. And to improve the segmentation performance of fuzzy based clustering approach, genetic algorithm and neural network techniques are also being used as supporting methods.

7.2 Future Work

In relation with the work done for this thesis and above conclusions obtained from it, future work may be addressed to the following points:

- Apart from simulated MRI images, synthetic images and more real MRI brain images should be used for testing. Use of more number and type of images will facilitate more reliable results and conclusions based on them.

- If MR image pre-processing is used before segmentation then it can improve segmentation results greatly. Since MR image pre-processing was out of scope of this thesis therefore it was not considered, but to obtain precise segmentation results from algorithms pre-processing in an unavoidable step.

- Improvement in the code of algorithms may improve the segmentation results, as efficient coding will result to efficient segmentation results.

- In case Improved fuzzy C-means (IFCM) algorithm, correct determination of earlier mentioned parameters can improve the segmentation results. As mentioned by authors of IFCM incorrect choice of parameters will worsen the results of segmentation. Therefore complete IFCM code will give proper results.

- In this thesis only classical and fuzzy based algorithms were used for comparisons, use of statistical algorithm like expectation maximisation algorithm will give more general and wider approach to the comparisons, displaying the ability of various techniques in segmenting complex and detailed medical images like MRI brain images.

REFERENCES

- Acton S. T. and Mukherjee D. P. (2000), "Scale space classification using area morphology," IEEE Transactions on Image Processing, vol. 9, no. 4, pp. 623-635.

- Bauer P., Nouak S. and Winker. R. (1996), "A brief course in fuzzy logic and fuzzy control," Retrieved from website: http://www.esru.strath.ac.uk/Reference/concepts/fuzzy/fuzzy.htm

- Bezdek J. C. (1981), Pattern recognition with fuzzy object function algorithms, Plenum press.

- BrainWeb (2006), Retrieved from http://www.bic.mni.mcgill.ca/brainweb/, website.

- BrainWeb (2006), "BrainWeb: Frequently Asked Questions with Answers," Retrieved from website: http://www.bic.mni.mcgill.ca/brainweb/faq.html

- Canon R. L., Dave J. V. and Bezdek J. C. (1986), "Efficient implementation of the fuzzy c-means clustering algorithms," IEEE Transactions on Pattern Analysis and Machine Intelligence, vol. PAMI-8, no. 2, pp. 248-255.

- Cheriet M., Said H. N. and Suen C. Y. (1998), "A recursive thresholding technique for image segmentation," IEEE Transactions on Image Processing, vol. 7, no. 6, pp. 918-920.

- Coleman G. B. and Andrews H. C. (1979), "Image segmentation by clustering," Proceedings of IEEE, vol. 67, no. 5, pp. 773-785.

- Collins D. L., Zijdenbos A. P., Kollokian V., Sled J. G., Kabani N. J., Holmes C. J. and Evans A. C. (1998), "Design and Construction of a Realistic Digital Brain Phantom," IEEE Transactions on Medical Imaging, vol. 17, no. 3, pp. 463-468.

- Corcosco C. A., Killlokian V., Kwan R. K. and Ewans A. C., (1997), "Brainweb: online Interface to a 3D MRI Simulated Brain Database," NeuroImage, vol. 5, no. 4, part 2/4, S425.

- Dave R. N. (1991), "Characterization and detection of noise in clustering," Pattern Recognition Letters, vol. 12, pp. 657-664.

- Douglas T. S. (1998), Imaging and Image Processing in Trans-femoral Prosthetics, PhD thesis, University of Strathclyde, UK.

- Dunn J. C. (1973), "A Fuzzy Relative of the ISODATA Process and Its Use in Detecting Compact Well-Separated Clusters," Journal of Cybernetics, vol. 3, pp. 32-57

- Dutta S. (1993), Knowledge Processing and Applied Artificial Intelligence. Butterworth-Heinemann, England.

- Ellard D. (2007), "History of MRI," Poster Presentation, Retrieved from University of Manchester, Clinical Radiology.
  http://www.isbe.man.ac.uk/personal/dellard/dje/about_me/about_me.htm

- EMRF Foundation (2003), "A short history of magnetic resonance imaging from a European point of view," Presentation, Retrieved from EMRF Online website:
  http://www.emrf.org/FAQs%20MRI%20History.html

- Fonar Corporation (2003), "MRI glossary," Retrieved from
  http://www.fonar.com/glossary.htm

- Geuns R., Wielopolski P., Bruin H., Rensing B., Ooijen P., Hulshoff M., Oudkerk M., and Feyter P. (1999), "Basic principles of Magnetic Resonance Imaging," Progress in Cardiovascular Diseases, Vol. 42, No. 2 (September/October), pp 149-156

- Gibbs P., Buckely D. L., Blackband S. J. and Horsman A. (1996), "Tumour volume determination from MR images by morphological segmentation," Physics in Medicine and Biology, vol. 41, pp. 2437-2446.

- Greenspan H., Ruf A., Goldberger J. (2006), "Constrained Gaussian mixture model framework for automatic segmentation of MR brain images," IEEE Transactions on Medical Imaging, vol. 25, no. 9, pp. 1233-1245.

- Hall L. O., Bensaid A. M., Clarke L. P., Velthuizen R. P., Silbiger M. S., and Bezdek J. C. (1992), "A comparison of neural network and fuzzy clustering techniques in segmenting magnetic resonance images of the brain," IEEE Transactions on Neural Networks, vol. 3, no. 5, pp. 672-682.

- Hesselink J. R. (2003), "Basic principles of MR imaging," Retrieved from University of California, Department of Radiology website: http://spinwarp.ucsd.edu/NeuroWeb/

- Hornak J. P. (1996-2007), "The basic of MRI," Retrieved from Rochester Institute of Technology, Centre for Imaging Science website:
  http://www.cis.rit.edu/htbooks/mri/inside.htm

- Kettaf F. Z., Bi D. and Beauvile J. P. (1996), "Comparison Study of Image Segmentation by Clustering Techniques," 3rd International Conference on Signal Processing, vol. 2, pp. 1280-1283, vol. 2.

- Krishnapuram R. and Keller J. M. (1993), "A positivistic Approach to Clustering," IEEE Transactions on Fuzzy Systems, vol. 1, no. 2, pp. 98-110.

- Kumar A., Welti D. and Renst R. R. (1978), "NMR Fourier Zeugmatography," Journal of Magnetic Resonance, vol. 18, pp 69-83.

- Kurtz L. and Benteftifa M. H. (1997), Analysis of Variance in Statistical Image Processing, Cambridge University Press.

- Kwan R. K. S., Evans A. C., Pike G. B. (1999), "MRI simulation-based evaluation of image processing and classification methods," IEEE Transactions on Medical Imaging, vol.18, no. 11, pp. 1085-1097.

- Law T. Y. and Heng P. A. (2000), "Automated extraction of bronchus from 3D CT images of lung based on genetic algorithm and 3D region growing," Proceedings of SPIE- Medical Imaging, vol. 3979, pp. 906-916.

- Lee C., Huh S., Ketter T. A. and Unser M. (1998), "Unsupervised connectivity-based thresholding segmentation of mid-sagittal brain MRI images," Computers in Biology and Medicine, vol. 28, no.3, pp. 309-338.

- Leemput K. V., Maes F., Vandermeulen D. and Suetens P. (1999), "Automated model-based tissue classification of MR images of the brain," IEEE Transactions on Medical Imaging, vol. 18, no. 10, pp. 897-908.

- Li C. L., Goldgolf D. B. and Hall L. O. (1993), "Knowledge- based classification and tissue labelling of MR images of human brain," IEEE Transactions on Medical Imaging, vol. 12, no. 4, pp. 740-750.

- Li J. and Gray R. M. (2000), Image Segmentation and Compression Using Hidden Markov Models, Kluwer Academic Publishers.

- Li W., Yushu L., Xinxin Z. and Yuanqing X. (2006), "Particle swarm optimisation for fuzzy c-means clustering," The Sixth World Congress on Intelligent Control and Automation, vol. 2, pp. 6055-6058.

- Liang Z. P. and Lauterbur P. (2000), Principles of Magnetic Resonance Imaging: A Signal Processing Perspective, IEEE Press Series in Biomedical Engineering.

- Lin Y., Tian J. and He. H. J. (2002), "Image Segmentation via fuzzy object extraction and edge detection and its medical application," Journals of X-ray science and Technology, vol. 10, pp. 95- 106.

- Lemieux L., Hagemann G., Krakow K., and Woermann F. G. (1999), "Fast, accurate and reproducible automatic segmentation of the brain in T_1–weighted volume MRI data," Magnetic Resonance in Medicine, vol. 42, pp. 127-135.

- Mackiewich B. (1995), Automatic segmentation of the brain in MRI, MSc thesis, Simon Fraser University, Retrieved from: http://www.cs.sfu.ca/~stella/grads.html

- MacQueen J. (1967), "Some methods of classification and analysis of multivariate observations," Proceedings of the Fifth Berkeley Symposium on Mathematical Statistics and Probability, vol. 1, pp. 281-297.

- Magnetic Resonance- Technology Information Portal (2007), Retrieved from: http://www.mr-tip.com/serv1.php?type=welcome

- Nyul L. G. and Udupa J. K. (1999), "On standardizing the MR image intensity scales," Magnetic Resonance Imaging, vol. 42, pp. 1072-1081.

- Pal N. R. and Pal S. K. (1993), "A review on image segmentation techniques," Pattern Recognition, vol. 26, no. 9, pp. 1277-1294.

- Pham D. L. and Prince J. L. (1999), "Adaptive fuzzy segmentation of magnetic resonance images," IEEE Transactions on Medical Imaging, vol. 18, no. 9, pp. 737-752.

- Pham D. L. (2001), "Spatial Models for Fuzzy Clustering," Computer Vision and Image Understanding, vol. 84, pp. 285-297.

- Pohle R. and Toennies K. D. (2001), "Segmentation of medical images using adaptive region growing," Proceedings of SPIE- Medical Imaging, vol. 4322.

- Powers D. (2002), "An introduction to EM algorithm," Retrieved from University of Texas at Austin, Liberal Arts Computer Lab website: http://www.la.utexas.edu/course-materials/sociology/soc386L/EM1.pdf

- Puddephat M. (2002), "Principles of magnetic resonance imaging," Retrieved from Easy Measure website magnetic resonance section:
http://www.easymeasure.co.uk/principlesmri.aspx

- Robb A. R. (2000), Biomedical Imaging, Visualization and Analysis, Wiley-Liss, Inc.

- Ruan C. (2003), "MRI artifacts: Mechanisms and Control," Retrieved from Research Imaging Centre UTHSCSA website:
http://ric.uthscsa.edu/personalpages/lancaste/DI2_Projects_2003/

- Savoy R. and Jovicich J. (2001), "MRI glossary," Retrieved from Massachutes Institute of Technology website:
http://web.mit.edu/hst.583/www/course2001/LECTURES/

- Shen S, Sandham W. and Granat M. (2003), "Preprocessing and segmentation of magnetic resonance imaging," Proc. 4th IEEE Annual International Conference on Information Technology Applications in Biomedicine, ITAB 2003, UK, pp. 149-152.

- Shen S. (2004), MRI brain tumour classification using image processing and data mining, PhD thesis, University of Strathclyde, UK.

- Shen S., Sandham W., Granat M. and Sterr A. (2005), "MRI fuzzy segmentation of brain tissue using neighborhood attraction with neural network optimization," IEEE Transactions on Information Technology in Biomedicine, vol. 9, no. 3, pp. 459-467.

- Siemens AG (2001), "MR glossary," Retrieved from Siemens Medical Solutions website: http://www.medical.siemens.com/siemens/en_US/gg_mr_FBAs/files/brochures/MR_Glossar _en.pdf

- Selvathi D., Arulmurgan A., Thamarai Seivi S. and Alagappan S. (2005), "MRI image segmentation using unsupervised clustering techniques," Sixth International Conference on Computational Intelligence and Multimedia Applications, pp. 105-110.

- Stelzer R. (2003), FuzzyWeb: A web Based Approach to Fuzzy System Design, BSc thesis, University of Derby, UK, Retrieved from website:
   http://wiki.atrox.at/images/d/d2/FYP_REPORT.pdf

- Suzuki H. and Toriwaki J. (1991), "Automatic segmentation of head MRI images by knowledge guided thresholding," Computerized Medical Imaging and Graphics, vol. 15, no.4, pp. 223-240.

- Taguchi G., Chowdury S. and Wu Y. (2000), The Mahanabolis-Taguchi System, McGraw-Hill Professional.

- Taheri, Ong and Chong (2007), "Threshold based 3-D tumor segmentation using level set (TSL)," Eighth IEEE Workshop on Applications of Computer Vision (WACV' 07), pp. 45.

- Tolias Y. A. and Panas S. M. (1998a), "On applying spatial constraints in fuzzy image clustering using a fuzzy rule-based system," IEEE Signal Processing Letters, vol. 5, no. 10, pp. 245-247.

- Tolias Y. A. and Panas S. M. (1998b), "Image segmentation by a fuzzy clustering algorithm using adaptive spatially constrained membership functions," IEEE Transactions on System, Man and Cybernet, Part A, vol. 28, no. 3, pp. 359-369.

- Wells, III W. M., Grimson W. E. L., Kikinis R. and Jolesz F. A. (1996), "Adaptive segmentation of MRI data," IEEE Transactions on Medical Imaging, vol. 15, no. 4, pp. 429-442.

- Zadeh L. A. (1965), "Fuzzy Sets," Information and Control, vol. 8, pp. 338-353.

- Westbrook C. and Kaut C. (1994), Handbook of MRI technique, Blackwell Science Ltd.

- Westbrook C. (2002), MRI at a Glance, Blackwell Publishing Ltd.

- Westbrook C. and Kaut C. (2002), MRI in practice, Second edition, Blackwell Publishing Ltd.

- Zhang Y. J. (1997), "Evaluation and Comparison of different segmentation algorithms," Pattern Recognition Letters, vol. 18, pp. 963-974.

APPENDIX I: LIST OF FIGURES

APPENDIX II: LIST OF TABLES

Numbering	Caption	Page
Table 2.1	Tissue brightness in MRI images	**13**
Table 6.1	Qualitative comparsions of algorithms	**59**
Table 6.2	Quantitative comparisons of algorithms	**62**

APPENDIX III: GLOSSARY

Axial: A plane, slice or section made by cutting the body or part of it at right angles to the long axis. If the body or part is upright, the cut would be parallel to the horizon.

Contrast: The relative difference of signal intensities in two adjacent regions of an image. Image contrast is heavily dependent on the chosen imaging technique (i.e., TE, TR, T_1), and is associated with such parameters as proton density and T_1 or T_2 relaxation times.

Coronal: A plane, slice or section made by cutting across the body from side to side and therefore parallel to the coronal suture of the skull.

Dipole: A magnetic field characterized by its own north and south magnetic poles separated by a finite distance

Euclidean distance: The straight line distance between two points. In a plane with p_1 at (x_1, y_1) and p_2 at (x_2, y_2), it is $\sqrt{(x_1 - x_2)^2 + (y_1 - y_2)^2}$

Frequency: The number of cycles or repetitions of any periodic wave or process per unit time. In electromagnetic radiation, it is usually expressed in units of hertz (Hz), where 1 Hz = 1 cycle per second.

Gauss: A unit of magnetic field strength that is approximately the strength of the earth's magnetic field at its surface (the earth's field is about 0.5 to 1G). The value of 1 gauss is defined as 1 line of flux per cm^2. As larger magnetic fields have become commonplace, the unit gauss (G) has been largely replaced by the more practical unit tesla (T), where 1 T = 10,000 G.

Hertz: The standard unit of frequency equal to 1 cycle per second. The larger unit megahertz (MHz) = 1,000,000 Hz.

Homogeneity: Uniformity of the main magnetic field.

Inhomogeneity: Lack of homogeneity or uniformity in the main magnetic field.

Noise: An undesirable background interference or disturbance that affects image quality.

Orthogonal: A plane or section perpendicular to the x-y-z coordinate system.

Quantum mechanics: Is a fundamental branch of physics with wide applications in experimental physics and theoretical physics that replaces classical mechanics and classical electromagnetism at the atomic and subatomic levels. Quantum mechanics is a more fundamental theory than Newtonian mechanics and classical electromagnetism, in the sense that it provides accurate and precise descriptions for many phenomena that these "classical" theories simply cannot explain on the atomic and subatomic level.

Radio Frequency: An electromagnetic wave with a frequency that is in the same general range as that used for the transmission of radio and television signals. Abbreviated as RF. The RF pulses used in MR are commonly in the 1-100 megahertz range, and their principle effect upon a body is potential tissue heating caused by absorption of the applied pulses of RF energy.

Receiver coil: A coil, or antenna, positioned within the imaging volume and connected to the receiver circuitry that is used to detect the NMR signal. In certain applications, the same coil can be used for both transmission and reception.

Resolution (Image resolution): Is the ability to differentiate neighbouring tissue structure. The higher the image resolution, the better small pathologies may be diagnosed.

Saggital: A plane, slice or section of the body cutting from front to back through the saggital suture of the skull, and continued down through the body in the same direction, dividing it into two parts, then turning one half to view it from its cut surface.

Signal to noise ratio (SNR): The ratio between the amplitude of the received signal and background noise, which tends to obscure that signal. SNR, and hence image quality, can be improved by such factors as increasing the number of excitations, increasing the field of view, increasing slice thickness, etc. SNR also depends on the electrical properties of the patient being studied and the type of receiving coil used.

Tesla (T): The preferred unit of magnetic flux density. One tesla is equal to 10,000 gauss. The Tesla unit value is defined as a field strength of 1 Weber/meter^2, where 1 Weber represents 1×10^8 flux lines.

Vector: A quantity that has both magnitude and direction and that is commonly represented by an arrow. The length of the line segment represents the magnitude,

and its orientation in space represents its direction. Vector quantities can be added to or subtracted from one another.

Voxel: Volume element; the element of the three-dimensional space corresponding to a pixel, for a given slice thickness.

References

All glossary definitions from:

- Fonar Corporation (2003), "MRI glossary", Retrieved from http://www.fonar.com/glossary.htm
- Siemens AG (2001), "MR glossary", Retrieved from Siemens Medical Solutions website: http://www.medical.siemens.com/siemens/en_US/gg_mr_FBAs/files/brochures/MR_Glossar_en.pdf
- Wikipedia (2007), "Wikipedia, The Free Encyclopedia", Retrieved from website: http://en.wikipedia.org/wiki/Main_Page

APPENDIX IV: COMPUTING DETAILS

- Personal computer hardware configuration: Intel Pentium Centrino processor, 2.0GB RAM

- Operating system: Windows XP, home edition

- Implementation software: MATLAB® 6.5

- Approximate number of lines of coding and execution time:

    Edge-based segmentation algorithm: 20 lines, time: 1 minute.

    K-means algorithm: 65 lines, time: 2 minutes.

    FCM algorithm: 80 lines, time: 4 minutes.

    IFCM algorithm: 100 lines, time: 5 minutes.

- An example of code is shown below:

```
lambda = 0.47;

epsln = 0.53;

nl = 1; % this controls the neighbourhood level for ease of programming for nl = 1
the actual neighbourhood level is 2, for nl2 =2 the actual neighbourhood level is 4

[newimag,V,u,nclust] = FCM;

[xsize,ysize] = size(newimag);

cluster = length(V);


counter = 0;                              %initialise main counter

unew = zeros(xsize,ysize,cluster);              %initialise new fuzzy values

unew1 = zeros(xsize,ysize,cluster);

while  counter < 2                        %set a limit on the counter
```

All details of the source code written in MATLAB® for this thesis can be found in accompanying CD.

APPENDIX V: SUMMARY OF THE PROJECT WORK

1. Preprocessing technique used: Normalisation of images was used prior to segmenting images.

2. Following segmentation algorithms were developed and used:

    a. Edge-based segmentation algorithm

    b. K-means clustering segmentation algorithm

    c. FCM clustering segmentation algorithm

    d. IFCM clustering segmentation algorithm

3a. Description: Synthetic images:

All synthetic images were obtained from "Brainweb website" with parameters: T_1, T_2, PD and Noise = 0% and 9% and artifact used was RF inhomogeneity of 0% and 40%.

3b. Description: Real images:

All real images for testing of this thesis were obtained from "Ballinger, MRI Tutor" website and "J. P. Hornak" website with parameters T_1, T_2, PD.

4. Input to the project:

A} Reviewed underlying MRI physics to understand image modalities (T_1, T_2, PD) and parameters depending on it.

B} Reviewed various segmentation techniques such as classical, fuzzy and reviewed algorithms based on these techniques, and developed algorithms namely 1) Edge-based segmentation, 2) K-means, 3) FCM, 4) IFCM in MATLAB®.

C} To see how algorithm is working, very initially they were tested with simple synthetic images, after which they were tested on simulated brain images (where ground truth was known).

D} For evaluating the algorithm their segmentation results were compared with two types of comparisons namely qualitative and quantitative. As described in

section 3 various modalities (T_1, T_2, PD) and parameters were used. Various modalities T_1, T_2, PD and parameters (such as noise, slice thickness, RF inhomogeneity artifact) combinations were used to observe the results of segmentation of 4 different algorithms.

E} Lastly qualitative comparison was alone with criteria such as

1. quality of segmentation results

2. time taken (computing time)

3. sensitivity to noise etc.

F} Quantitative comparison was done with following criterion

Segmentation results of original image were compared with original image (since ground truth was known). Quantitative evaluation was done by counting the correctly and incorrectly segmented pixels in segmented image. For categorising pixels two criteria were used a) correct segmentation and b) incorrect segmentation.

APPENDIX VI: CONTENTS OF ACCOMPANYING CD

Details of contents of the accompanying CD are mentioned below.

1. First folder contains poster/presentations made (in initial stage) for this thesis.

2. Second folder contains copy of complete thesis in Microsoft word format.

3. Third folder contains source code of all the algorithms developed in MATLAB$^{\circledR}$ for this thesis.

Following is the list of algorithms written and developed for this thesis.

a. Edge-based segmentation algorithm.

b. K-means clustering segmentation algorithm

c. Fuzzy C-means clustering segmentation algorithm

d. Improved fuzzy C-means clustering segmentation algorithm

e. Algorithm for image standardisation

f. Algorithm for quantitative comparison